How to cite: *Angew. Chem. Int. Ed.* **2022,** *61*, e202213026
International Edition: doi.org/10.1002/anie.202213026
German Edition: doi.org/10.1002/ange.202213026

Metal-Air Batteries

Light-Assisted Metal–Air Batteries: Progress, Challenges, and Perspectives

Jiaxin Li, Kun Zhang, Bingjie Wang, and Huisheng Peng**

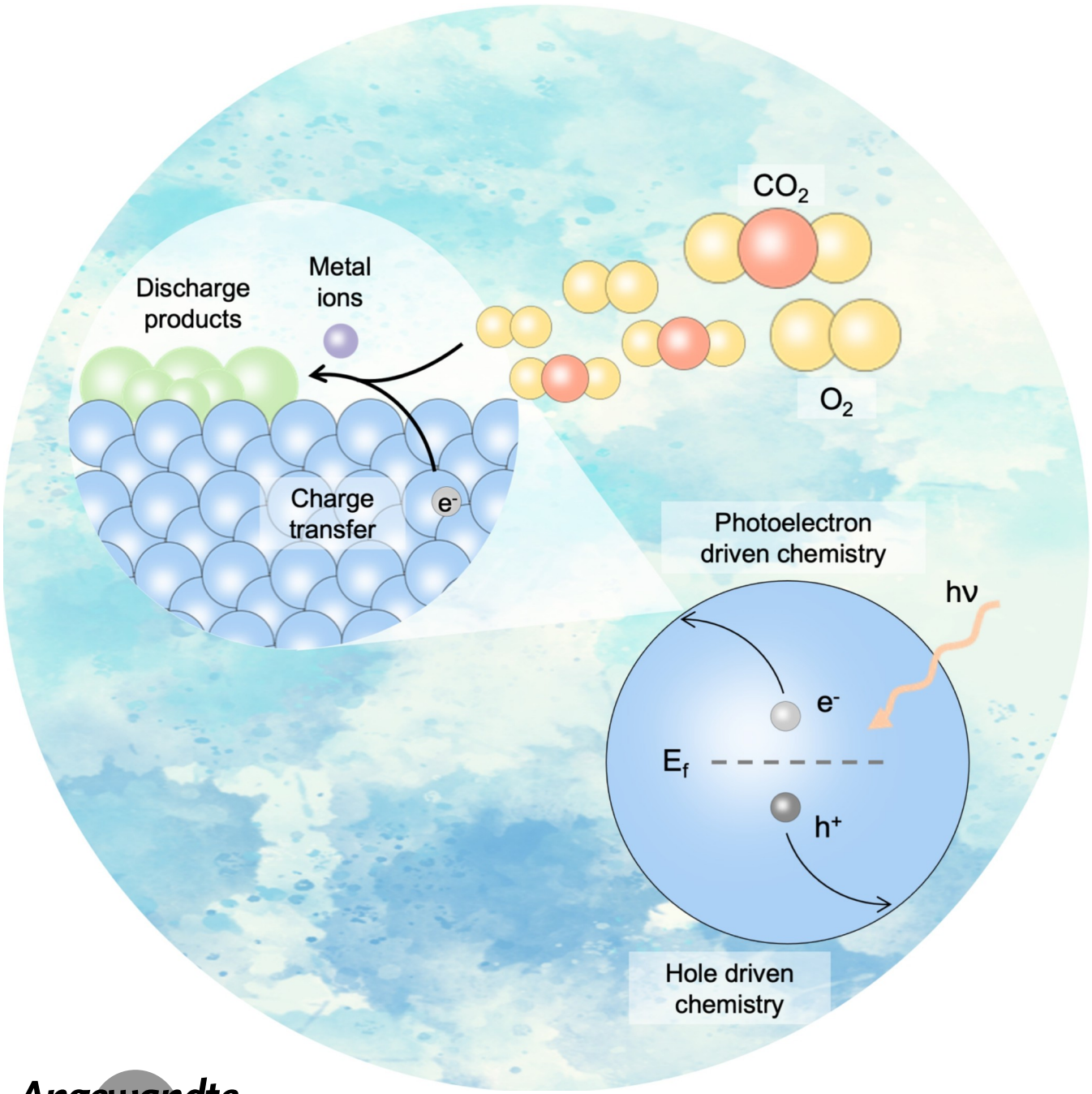

Abstract: Metal–air batteries are considered one of the most promising next-generation energy storage devices owing to their ultrahigh theoretical specific energy. However, sluggish cathode kinetics (O_2 and CO_2 reduction/evolution) result in large overpotentials and low round-trip efficiencies which seriously hinder their practical applications. Utilizing light to drive slow cathode processes has increasingly becoming a promising solution to this issue. Considering the rapid development and emerging issues of this field, this Review summarizes the current understanding of light-assisted metal–air batteries in terms of configurations and mechanisms, provides general design strategies and specific examples of photocathodes, systematically discusses the influence of light on batteries, and finally identifies existing gaps and future priorities for the development of practical light-assisted metal–air batteries.

1. Introduction

Constantly increasing energy needs and environmental awareness have accelerated the transition from traditional fossil fuels to clean renewable energy, especially for the generation of electric energy. Various anticipated application scenarios, such as portable electronics, electric vehicles, and interstellar travel, also have already put forward higher requirements for the necessary power supply systems. These increasing demands make the mission of designing new high-specific-energy batteries more urgent than ever before. Lithium-ion (Li-ion) batteries have dominated the rechargeable batteries market and have gradually penetrated every aspect of our daily life since their commercialization in the late 1990s.[1] At present, Li-ion batteries have gradually approached their theoretical specific energy (387 $Wh\,kg^{-1}$).[2] In the long run, although fully optimized, Li-ion battery chemistry still cannot meet the needs for higher energy densities owing to its inherent limitations.[3,4] This thus motivates intense research activities in alternative next-generation energy storage devices.

Among various candidates, metal–air batteries are receiving intense interest since their theoretical specific energy is 3–10 times higher than that of commercialized Li-ion batteries.[3,5–8] The Li–O_2 battery gets the most attention because its specific energy ($\approx$3500 $Wh\,kg^{-1}$) and output voltage ($\approx$2.96 V) are the highest among non-aqueous batteries. The Li–CO_2 battery also has aroused rising attention because it can fix CO_2 and store energy to alleviate the greenhouse effect and energy crisis.[9–11] Among the aqueous batteries, the Zn–air battery captures the most interest by virtue of its high specific energy ($\approx$1086 $Wh\,kg^{-1}$) and superior stability and low cost of the Zn anode.

Despite great prospects, current metal–air batteries are far from satisfactory, with poor electrochemical performances. Theoretically, O_2 (CO_2) can be reduced and released reversibly during discharging and charging of metal–air batteries. The battery then produces an output voltage depending on the theoretical potential difference between the air cathode and metal anode. However, O_2 (CO_2) reduction/evolution reactions (ORR/OER and CO_2RR/CO_2ER) during discharging/charging often proceed with high overpotentials and low round-trip efficiencies. Therefore, electrocatalysts or electrolyte additives are always needed to accelerate the cathode processes. In the past years, considerable efforts have been made on developing new cathode electrocatalysts[11–14] (e.g., noble metals,[15–17] metal oxides/sulfides,[18] and carbon materials[19–21]) and soluble redox mediators (e.g., lithium halides,[22–24] tetrathiafulvalene,[25] and 2,2,6,6-tetramethylpiperidinyloxyl[26]). However, it is still difficult to obtain catalysts to facilitate the discharge/charge process effectively and the large polarized voltages remain. The poor selectivity of catalysts and the inevitable migration of soluble mediators to the anode part result in serious side reactions, impeding the lifetime of the battery.[27] Moreover, many cathode electrocatalysts and electrolyte mediators are unrealistic and unsustainable because of expensive reactants, complex synthesis, and low yields. Therefore, it is necessary to propose new strategies to tackle the above issues.

In 2014, the first light-assisted Li–O_2 battery was constructed by integrating an extra redox shuttle-coupled dye-sensitized TiO_2 photoelectrode as the third electrode into a conventional Li–O_2 battery.[28] Under illumination, the charge voltage was sharply decreased to 2.72 V. Instantly, this pioneering study provided a new paradigm and inspired peer researchers to address the problems of metal–air batteries with light. Gradually, utilizing light to drive slow ORR/OER (CO_2RR/CO_2ER) has emerged as an increasingly popular strategy to achieve high-efficiency metal–air batteries. By designing novel semiconductor photocatalysts matched with the targeted battery chemistry, researchers have successfully constructed light-assisted Li–O_2 (air), Li–CO_2, zinc–air (Zn–air), and sodium–air (Na–air) batteries, and record-high electrochemical performances are still being achieved based on advances in materials and structures (Figure 1). Photothermal materials also have been introduced to the cathodes to accelerate battery reactions by converting light into heat. In addition to developing new materials and devices, researchers have gradually gained a deeper understanding of light-involved cathode reactions. The light-assisted strategy effectively improves the performance of metal–air batteries and also provides a new method of utilizing and storing photoenergy. In contrast to conven-

[*] J. Li, K. Zhang, Prof. B. Wang, Prof. H. Peng
State Key Laboratory of Molecular Engineering of Polymers
Department of Macromolecular Science
and Laboratory of Advanced Materials, Fudan University
Shanghai 200438 (P. R. China)
E-mail: wangbingjie@fudan.edu.cn
penghs@fudan.edu.cn
J. Li
Department of Colloid Chemistry
Max Planck Institute of Colloids and Interfaces
14476 Potsdam (Germany)

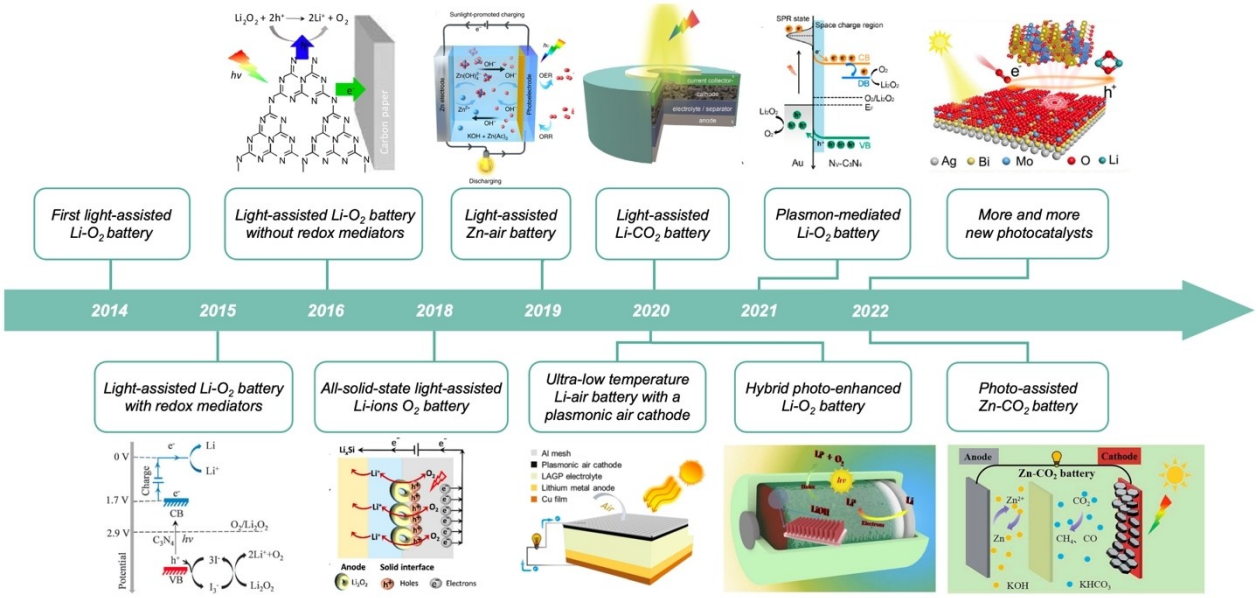

Figure 1. Brief chronology of the development of light-assisted metal–air batteries. Reproduced with permission.[51–60] Copyright 2016, 2020, 2022 Royal Society of Chemistry. Copyright 2018, 2020, Elsevier. Copyright 2019, Macmillan Publishers Ltd. Copyright 2020, 2022 Wiley-VCH. Copyright 2021, National Academy of Sciences of the United States of America.

tional integration systems including independent energy models (solar cells, batteries, and supercapacitors) and complex connections, photoenergy is directly converted to electric energy and then to chemical energy stored in the light-assisted metal–air battery. Despite significant progress, many issues still exist waiting to be solved for the new energy storage systems.

Several reviews have been published in which the configurations and working principles of light-assisted batteries are briefly introduced.[29–36] For example, the applications of solar energy in different rechargeable batteries were summarized in 2017,[29] and the advancements in integrated photovoltaic–battery systems in two/three-electrode configurations were presented in 2018.[30] Further, the structures,

Jiaxin Li received her B.S. degree in Polymer Materials and Engineering from Northwestern Polytechnical University (Xi'an, China) in 2018 and her M.S. degree from Fudan University (Shanghai, China) under the supervision of Prof. Bingjie Wang and Prof. Huisheng Peng in 2021. She is now a Ph.D. candidate in the Colloid Chemistry Department, Max Planck Institute for Colloids and Interfaces (Potdam, Germany). She focuses on the synthesis of carbon materials and their applications in metal–air batteries and capacitors.

Kun Zhang received his B.S. degree in Polymer Materials and Engineering from Nanjing University of Science and Technology (China) in 2020. He is now pursuing his M.S. degree at Fudan University under the supervision of Prof. Bingjie Wang and Prof. Huisheng Peng. He focuses on the synthesis of organic electrode materials and their applications in flexible fiber batteries.

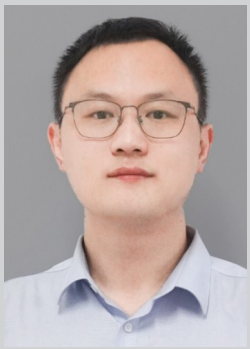

Bingjie Wang is currently Associate Professor at the Laboratory of Advanced Materials at Fudan University. He received his B.E. degree in Polymer Materials at Sichuan University (Chengdu, China) in 2009 and Ph.D. degree from Ningbo Institute of Materials Technology and Engineering, Chinese Academy of Science in 2014. He has been worked in Prof. Huisheng Peng's group at Fudan University since 2014. He focuses on the fabrication and industrialization of flexible energy storage devices.

Huisheng Peng is currently Professor at Department of Macromolecular Science and Laboratory of Advanced Materials at Fudan University. He received his B.E. degree in Polymer Materials at Donghua University (Shanghai, China) in 1999, his M.S. degree in Macromolecular Chemistry and Physics at Fudan University in 2003, and his Ph.D. degree in Chemical Engineering at Tulane University (New Orleans, USA) in 2006. He then worked at Los Alamos National Laboratory before joining Fudan University in 2008. He focuses on the new direction of fiber electronics.

operating principles, and electrochemical performances of light-responsive batteries have been summarized and analyzed.[32,33] The above reviews provide a comprehensive introduction to various light-assisted energy-storage devices (e.g., Li-ion, Li–iodine, Li–S, Li–O_2 batteries, etc.), but rarely discuss the unique structures and properties of light-assisted metal–air batteries. Recently, an inspiring tutorial review introduced the fundamental photoelectrochemical process of O_2 in the Li–O_2 battery,[36] but did not discuss Li–CO_2 and Zn–air batteries. So far, the configurations and properties of light-assisted metal–air batteries have not been carefully reviewed, and the challenges and outlooks in this rising field have not been systematically discussed.

In this Review, we will first introduce the typical configurations and working principles of light-assisted metal–air batteries. Then, the design strategies and the latest examples of photocathodes will be summarized and analyzed from the perspective of materials. We will further systematically discuss the positive and negative influences of illumination on the metal–air battery. Finally, the key challenges and future perspectives for light-assisted metal–air batteries will be discussed. This Review aims to summarize the basic knowledge of the promising devices as innovative paradigms and inspire more researchers to find ways to create better light-assisted metal–air batteries.

2. Configurations and Principles

In this section, the fundamental principles of the photoelectrochemical process will be first introduced. Then, the typical configurations and working mechanisms of regular and light-assisted Li–O_2 (CO_2) and Zn–air batteries via the photoelectric effect will be discussed in detail. Light-assisted metal–air batteries via the photothermal effect will also be briefly introduced as a supplement.

2.1. Basics of Photochemistry

Photochemistry encompasses photon-driven reaction processes including light absorption, charge carrier separation, and reduction/oxidation reactions. The photocatalytic mechanism of a single-component semiconductor photocatalyst mainly involves the following steps: When photocatalyst absorbs incident photons with energy equal to or higher than its band gap energy E_g (also called the forbidden band gap), the electrons in the valence band (VB) are excited to the conduction band (CB), leaving the holes in the VB. The photoelectrons in the CB are involved in the reduction reaction, while holes in the VB participate in the oxidation reaction. The band gap and CB/VB positions determine the light absorption property and redox capability of semiconductors, respectively. After charge carrier separation, photoelectrons and holes undergo the following three possible processes: 1) they migrate to the surface of the photocatalyst to drive the reduction or oxidation reaction; 2) they recombine and are converted to heat or photons; 3) they are captured by defect sites. Generally, around 90 % of photoelectrons and holes recombine after separation, while less than 10 % of separated carriers are involved in photocatalytic reactions.[37] The full harvest of solar energy and effective separation of photogenerated carriers are vital in promoting photocatalytic efficiency. An ideal photocatalyst is expected to have broad light absorption, a suitable band structure for the target redox reactions, rapid carrier transfer, and efficient carrier separation. Many strategies have been proposed to design better photocatalysts, such as changing morphology/crystallinity, introducing defects, and building junctions (heterojunctions, Schottky junctions, and phase junctions). The photon-driven reactions of photocatalysts have realized many meaningful applications, such as water splitting, CO_2 reduction, and pollutant decomposition.[38–41]

2.2. Basics of Metal–Air Batteries

A typical metal–air battery consists of a metal anode, an electrolyte (separator), and a porous air cathode. The electricity is generated by the redox reactions between the metal anode and the air cathode. Depending on the type of electrolyte, metal–air batteries are divided into non-aqueous and aqueous systems, in which non-aqueous Li–O_2 and aqueous Zn–air batteries receive the most research interest due to their high theoretical specific energy.[42–47] The non-aqueous Li-CO_2 battery has a similar configuration and working mechanism to a Li–O_2 battery.[48,49] The working mechanisms for typical Li–O_2, Li–CO_2, and Zn–air batteries are described by the following equations.

$$2\,Li + O_2 \rightleftharpoons Li_2O_2 \quad E^0 = 2.96\ V$$

$$4\,Li + 3\,CO_2 \rightleftharpoons 2\,Li_2CO_3 + C \quad E^0 = 2.80\ V$$

$$2\,Zn + O_2 \rightleftharpoons 2\,ZnO \quad E^0 = 1.65\ V$$

For typical aprotic Li–O_2 (CO_2) battery, O_2 (CO_2) molecules from the surrounding atmosphere diffuse and dissolve into the electrolyte; O_2 (CO_2) captures electrons from the external circuit, combines with Li^+ ions in the electrolyte, and forms solid discharge products at the porous air cathode during discharging. These products are expected to undergo oxidative decomposition and release O_2 (CO_2) in a thermodynamically reversible way during charging. For a rechargeable Zn–air battery, O_2 is reduced to OH^- at the air cathode and migrates to the Zn anode, where it reacts in the alkaline electrolyte to generate $Zn(OH)_4^-$ which then becomes insoluble ZnO at the anode as the process proceeds during discharging. During charging, ZnO is reduced to metallic Zn at the anode while the oxidation of OH^- to O_2 takes place at the cathode. Metal–air batteries often suffer from large overpotentials and low energy efficiencies owing to sluggish ORR/OER (CO_2RR/CO_2ER) processes; thus, electrocatalysts or electrolyte additives are necessary to promote the discharge and charge processes of metal–air batteries. A few reviews have discussed the design strategies of cathode electrocatalysts.[4,45,50]

2.3. Basics of Light-Assisted Metal–Air Batteries

The first light-assisted Li–O_2 battery comprised an extra photoelectrode and redox mediator in the electrolyte.[28] The three-electrode configuration suffers from complex fabrication and operation, low safety, and high cost, while redox mediators can aggravate parasitic reactions including anode corrosion and electrolyte decomposition. Hence, the light-assisted metal–air battery in a two-electrode configuration (photocathode as photoelectrode and air cathode simultaneously) without redox mediators has become the major research paradigm. In this review we will focus on light-assisted metal–air batteries in the two-electrode configuration. Depending on the photoactive materials at the cathodes, the light-assisted mechanisms include photoelectric and photothermal effects.

The configuration of a light-assisted metal–air battery via the photoelectric effect is similar to that of a regular metal–air battery, and mainly consists of a metal anode, an electrolyte, and a porous cathode with photocatalysts. The band structure of the photocatalyst should be designed toward the target battery chemistry. The VB potentials of photocatalysts should be lower than the oxidation potential of O_2/Li_2O_2 for a non-aqueous Li–O_2 battery, $CO_2/(Li_2CO_3 + C)$ for a non-aqueous Li–CO_2 battery, or O_2/OH^- pairs for an aqueous Zn–air battery. Correspondingly, the excited electrons in the CB should show a higher chemical potential than the equilibrium potentials of metal–air batteries, namely a stronger reduction activity.

The working mechanisms of light-assisted Li–O_2 (CO_2) and Zn–air batteries are shown in Table 1 and Figure 2. Under illumination, photocatalysts harvest photons of suitable energy and generate numerous photoelectrons/holes of certain energy levels to promote the discharge/charge reactions. For Li–O_2 (CO_2) batteries, O_2 (CO_2) molecules from the environment first diffuse through the photocathode and dissolve into the electrolyte. Then, the adsorbed O_2 (CO_2) molecules at the photocathode are reduced by photoelectrons, combine with Li^+ in the electrolyte, and are transformed into the discharge products Li_2O_2 ($Li_2CO_3 + C$) after several intermediate steps. Meantime, the holes are neutralized with the electrons from the external circuit. During the subsequent charging process, the holes oxidize solid products and release O_2 (CO_2) at a plus potential, and the electrons migrate to the external circuit. Similarly, the photocathode harvests photons and generates electron–hole pairs for the Zn–air battery. O_2 is reduced by the excited photoelectrons to OH^- in an alkaline electrolyte, accompanied by the electrochemical oxidation of Zn to Zn^{2+}. In a reverse charging process, the holes migrate to the photocathode to oxidize H_2O to O_2, and photoelectrons rapidly migrate to the external circuit, accompanied by the reduction of $Zn(OH)_4^{2-}$ to Zn and OH^-.

Note that the above discussion assumes that the photocatalysts can simultaneously enhance discharge and charge processes. Nevertheless, many photocatalysts only promote either the discharge or charge process depending on the n-type/p-type nature of the semiconductors. Here, it should be noted that although the theoretical discharge and charge voltages of a light-assisted battery are equal to the VB and CB potentials of photocatalysts in values, the two concepts are different in physical nature. The former is the potential difference between Li^+/Li (or ZnO/Zn) couples and the redox pairs at the cathode, while the latter is the intrinsic electronic energy state of photocatalysts, demonstrating the thermodynamic feasibility of photoelectrons/holes for accelerating cathode reactions. In addition to the photoelectric materials, integrating photothermal materials into cathodes also provides a feasible strategy to enhance cathode kinetics and broaden operating temperature by absorbing photons to warm up the battery in order to reduce internal resistances, enhance interfaces, and accelerate kinetics.

The main differences between regular and light-assisted batteries lie in the design of cathodes and setup. Cathode electrocatalysts in conventional metal–air batteries mediate electrochemical reaction pathways and decrease energy barriers mainly depending on their intrinsic chemical structures. Due to the limited chemically driven force for the cathode reactions, the discharge/charge voltages of regular metal–air batteries are much lower/higher than the theoretical equilibrium voltages, generating large overpotentials. In contrast, with the photocoupled reaction pathways, the actual discharge/charge voltages of light-assisted batteries sometimes can be higher/lower than the thermodynamic equilibrium limit of batteries, which is attributed to the participation of photoelectrons/holes in the cathode reactions. Therefore, light-assisted batteries can achieve much higher round-trip efficiencies (even higher 100%) than conventional devices. However, light-assisted batteries have higher demands for packaging and setup. Now, at a lab scale, researchers already pay more for the special coin cells with light-transmitting cathodes, the transparent sealed testing boxes, light sources, and temperature control devices. In

Table 1: Working mechanisms of representative light-assisted metal–air batteries.

		Li–O_2 battery Photocatalyst $\xrightarrow{hv}$ $e^-_{hv} + h^+_{hv}$	Li–CO_2 battery	Zn–air battery
Discharge	Anode	$Li \rightarrow Li^+ + e^-$	$Li \rightarrow Li^+ + e^-$	$Zn + 4OH^- \rightarrow Zn(OH)_4^{2-} + 2e^-$ $Zn(OH)_4^{2-} \rightarrow ZnO + H_2O + 2OH^-$
	Photocathode	$O_2 + 2e^-_{hv} + 2Li^+ \rightarrow Li_2O_2$	$4Li^+ + 3CO_2 + 4e^-_{hv} \rightarrow 2Li_2CO_3 + C$	$O_2 + 4e^-_{hv} + 2H_2O \rightarrow 4OH^-$
	Overall	$2Li + O_2 \rightarrow Li_2O_2$	$4Li + 3CO_2 \rightarrow 2Li_2CO_3 + C$	$2Zn + O_2 \rightarrow 2ZnO$
Charge	Anode	$Li^+ + e^- \rightarrow Li$	$Li^+ + e^- \rightarrow Li$	$Zn(OH)_4^{2-} + 2e^- \rightarrow Zn + 4OH^-$
	Photocathode	$Li_2O_2 + 2h^+_{hv} \rightarrow O_2 + 2Li^+$	$2Li_2CO_3 + C + 4h^+_{hv} \rightarrow 4Li^+ + 3CO_2$	$4OH^- + 4h^+_{hv} \rightarrow O_2 + 2H_2O$
	Overall	$Li_2O_2 \rightarrow 2Li + O_2$	$2Li_2CO_3 + C \rightarrow 4Li + 3CO_2$	$2ZnO \rightarrow 2Zn + O_2$

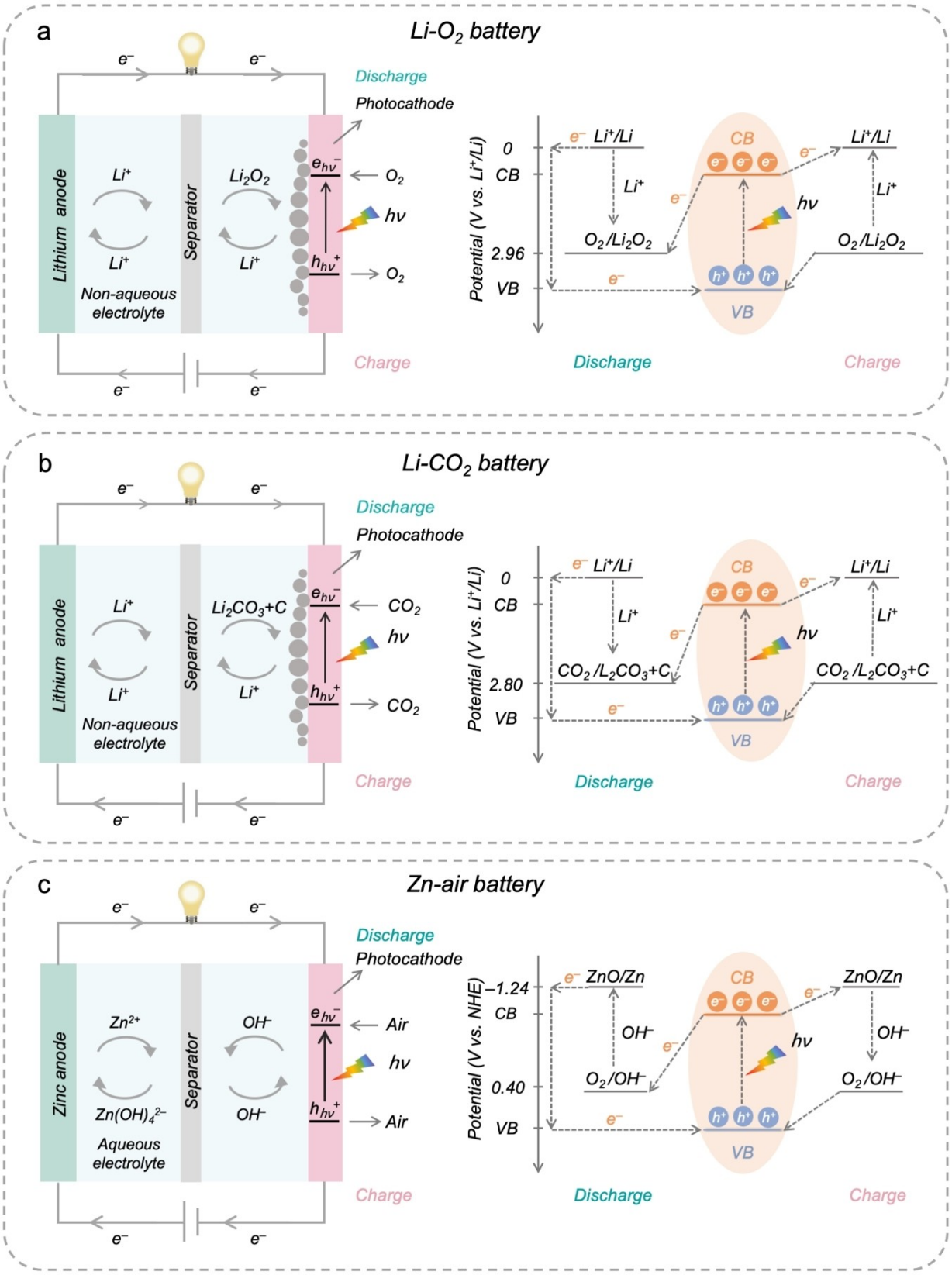

Figure 2. Schematic illustrations of device configurations and working mechanisms of light-assisted a) non-aqueous Li-O_2, b) Li-CO_2, and c) aqueous Zn-air batteries.

comparison, conventional metal–air batteries cost less in the packaging and testing process.

3. Design of Photocathodes

Photocathodes are vital in harvesting and utilizing photoenergy to boost the performance of light-assisted metal–air batteries. A photocathode, in general, comprises a photocatalyst and a current collector (e.g., carbon paper/cloth, metal mesh/foam/fiber, and conductive glasses). At an early stage, single-component photocatalysts (e.g., C_3N_4, Fe_2O_3) were directly deposited at a current collector as a photocathode. Subsequently, more enhanced designs have been proposed to overcome the limited light absorption and severe carrier recombination of single photocatalysts. Representative photocatalysts include metal oxides (e.g., TiO_2, WO_3, Fe_2O_3, Cu_2O, and Co_3O_4), metal sulfides (e.g., ZnS, MoS_2, $ZnIn_2S_4$, and In_2S_3), carbon nitrides (e.g., C_3N_4, C_4N), polymers (e.g., pTTh, PBTD, and metal–organic polymers), and their derivatives. Photothermal materials (e.g., Ru, RuO_2, Ag, and Au) also have been integrated into the air cathodes. So far, various light-assisted metal–air batteries have been constructed with significant progress (e.g., Li–O_2, Li–CO_2, Zn–air, Zn-CO_2, and Al–air batteries). Table 2 shows the configurations and properties of representative light-assisted metal–air batteries based on various photocathodes.

In addition to meeting requirements similar to those of regular air cathodes (electrocatalysts), such as porous structures, high catalytic activity, and decent chemical/electrochemical stability, the photocatalysts should also fulfill the following criteria for efficient photoenergy utilization: They should 1) possess large photocatalytically active areas to absorb light; 2) have a broad light absorption to make full use of the solar spectrum; 3) exhibit efficient separation and transfer of charge carriers; and 4) show high resistance for photocorrosion. In this section, we first provide fundamental design principles for photocatalysts and then introduce specific applications in light-assisted metal–air batteries.

3.1. Design Strategies for Photocatalysts

3.1.1. Enlarging the Active Surface

For conventional aprotic Li–O_2 (CO_2) batteries, cathode catalysts with larger active surfaces are favorable for the deposition and decomposition of solid discharge products for high capacity and enhanced reversibility. In the light-assisted battery, the morphology and structure of the photocatalysts is also important, as it also directly influences photon absorption, carrier generation, and subsequent photoelectrochemical reactions. It is common to deposit nanostructured photocatalysts on a three-dimensional current collector as the photocathode of a photoinvolved metal–air battery to to increase access to the active surface of the photocatalyst.[95] Various nanostructures have been reported with rich reactive surfaces (e.g., nanowires, nanorods, nanotube arrays),[61,83,84] while introducing a second component (e.g., metal nanoparticles) to the first photocatalyst is also feasible to unlock more active surfaces.[58,83]

3.1.2. Widening Light Absorption

The photoelectrochemical processes of light-assisted metal–air batteries are initiated by light absorption, which is determined by the band structure of the semiconductor. Most semiconductors mainly absorb light in the ultraviolet and near-ultraviolet regions ($E_g \approx 3.0$ eV, wavelength < 413 nm), which make up only about 7 % of the entire solar spectrum. To make the most of the solar spectrum, the following strategies can be adopted: 1) band structure engineering, which means developing narrow band gap semiconductors to enable the absorption of visible light ($E_g < 3.0$ eV), and 2) dye sensitization, which refers to using dye molecules to absorb visible light and generate more charge carriers.

Band structure engineering. Many efforts have been devoted to developing narrow band gap semiconductors for visible-light utilization. Distinct from TiO_2 ($E_g \approx 3.0$ eV), WO_3 shows extensive visible-light response ($E_g \approx 2.5$–2.8 eV), good electron mobility, and short hole diffusion length, which enabled a visible-light-responsive Li–O_2 battery.[65] α-Fe_2O_3 ($E_g \approx 1.9$–2.2 eV) was used in a light-assisted Zn–air battery and a hybrid Li–O_2 battery ($O_2 + 4\,Li + 2\,H_2O \rightleftharpoons 4\,LiOH$).[51,52] Spinel-type Co_3O_4 ($E_g \approx 1.5$–2.2 eV) worked as a bifunctional photocatalyst toward ORR/OER in a Zn–air battery.[90] C_4N ($E_g = 1.99$ eV) enabled a Zn–air battery capable of harvesting visible light.[95]

Dye sensitization. Dye sensitization is an efficient strategy to extend light absorption and has been widely applied in solar cells. Visible light is initially captured by the dye molecules adsorbed on the surface of the semiconductor. The photogenerated charge carriers are excited in the dye molecules and injected into the energy level of the semiconductor, while the excited dye molecules can recover to the initial state by reacting with a redox mediator. The first light-assisted Li–O_2 battery was constructed using an N719 dye-sensitized TiO_2 photoelectrode with the I^-/I_3^- redox couple.[28] This strategy has hardly been used in recent photocathodes probably because of the high cost of the dye molecules and tedious experimental steps.

3.1.3. Enhancing Carrier Separation

Extending light absorption increases the concentration of photogenerated electron–hole pairs, while achieving effective carrier separation is also vital for efficient photoenergy utilization in the photoelectrochemical process. Many strategies have been proposed to separate the photogenerated electron–hole pairs, such as introducing defect energy levels and building junctions, including heterojunction and Schottky junction.

Table 2: Configurations and properties of representative light-assisted metal–air batteries.

Type	Photocathode Photocatalyst	Current collector	Electrolyte	Light source	Current density [$mA\,cm^{-2}$]	Cut-off capacity [$mAh\,cm^{-2}$]	Discharge voltage [V]	Charge voltage [V]	Round-trip efficiency 1st [%]	Cycle	Refs.
Li-O_2 (air)	TiO_2/N719	Ti gauze	$LiClO_4$/LiI/DMSO	AM 1.5	0.016	0.016	–	2.72	–	4	[28]
	Defective TiO_2	Carbon textile	$LiClO_4$/TEGDME	300 W Xe lamp	0.02	0.02	2.65	2.86	92.6	30	[61]
	TiO_2–Fe_2O_3	Carbon cloth	$LiCF_3SO_3$/TEGDME	500 W Xe lamp	0.01	0.01	3.06	3.24	94.4	100	[62]
	TiN/TiO_2	Carbon cloth	$LiCF_3SO_3$/TEGDME	AM 1.5	200 $mA\,g^{-1}$	1000 $mAh\,g^{-1}$	2.75	2.94	93.5	/	[63]
	TiO_2–Au	Ti mesh	$LiCF_3SO_3$/TEGDME	1000 W Xe lamp	333 $mA\,g^{-1}$	500 $mAh\,g^{-1}$	≈2.37	≈2.75	≈86	200	[64]
	WO_3	Carbon textile	$LiClO_4$/TEGDME	300 W Xe lamp	0.06	0.06	2.71	3.63	74.6	100	[65]
	α-Fe_2O_3	FTO	LAGP/LiCl/LiOH/H_2O	300 W Xe lamp	0.12	0.12	2.57	3.13	82.1	45	[52]
	α-Fe_2O_3 /NiOOH	FTO	LAGP/LiCl/LiOH/H_2O	AM 1.5	0.12	0.12	2.64	3.03	87.1	150	[66]
	$LaFeO_3$	FTO	LiTFSI/TEGDME/ LAGP/LiCl/LiOH	–	0.02	0.04	3.24	3.49	93.1	80	[67]
	ZnS@MWCNT	Hydrophobic carbon paper	LiTFSI/TEGDME	XEF-501S Xe lamp	100 $mA\,g^{-1}$	500 $mAh\,g^{-1}$	–	2.20	–	150	[68]
	ZnS@CNT	Carbon paper	LiTFSI/SCN	XEF-501S Xe lamp	0.026	0.026	–	2.08	–	50	[53]
	CdSe/ZnS QD@CNT	Stainless-steel foam	LiTFSI/TEGDME	500 W Xe lamp	100 $mA\,g^{-1}$	100 $mAh\,g^{-1}$	≈2.70	≈3.70	≈73	30	[69]
	MoS_2/$ZnIn_2S_4$	Carbon paper	LiTFSI/TEGDME	300 W Xe lamp	0.05	0.05	3.18	3.29	96.7	65	[70]
	$BiVO_4$	FTO	LAGP/LiCl/LiOH/H_2O	300 W Xe lamp	0.12	0.12	2.44	3.26	74.8	6	[52]
	$CeVO_4$@CNT	Carbon paper	LiTFSI/TEGDME	Xe lamp	0.15	0.15	2.50	3.48	71.8	50	[71]
	g-C_3N_4	Carbon paper	$LiClO_4$/LiI/TEGDME	XEF-501S Xe lamp	0.01	0.01	2.73	1.90	142	50	[56]
	g-C_3N_4	Carbon paper	LiTFSI/TEGDME	XEF-501S Xe lamp	0.01	0.01	2.74	1.96	140	70	[57]
	C_3N_4	Carbon paper	$LiClO_4$/TEGDME	400 W UV lamp	0.04	0.20	3.22	3.38	95.3	10	[72]
	Au/N_V-C_3N_4	Carbon paper	LiTFSI/TEGDME	300 W Xe lamp	0.05	0.25	3.16	3.26	97.0	50	[58]
	$CoSe_2$@g-C_3N_4	Carbon paper	$LiClO_4$/DMSO	Solar light 100 $mW\,cm^{-2}$	0.30	0.25	≈2.75	≈3.75	≈73	/	[73]
	Fe_2O_3/C_3N_4	Carbon paper	LiTFSI/TEGDME	300 W Xe lamp	0.10	0.20	3.13	3.19	98.1	50	[74]
	Co-TABQ	Carbon paper	LiTFSI/TEGDME	300 W Xe lamp	0.10	0.50	3.12	3.32	94.0	50	[75]
	pTTh	Carbon paper	LiI/LiTFSI/TEGDME	300 W Xe lamp	0.02	0.02	3.10	3.19	97	150	[76]
	$CsPbBr_3$@PCN-333(Fe)	Carbon paper	LiTFSI/TEGDME	–	0.01	0.01	3.19	3.44	92.7	100	[77]
	(4,4′-EDP) Pb_2Br_6	Carbon nanosponge	LiTFSI/TEGDME	500 W Xe lamp	0.01	0.01	2.91	3.42	85.1	170 h	[78]
	Siloxene nanosheets	Ni foam	LiTFSI/TEGDME	500 W Xe lamp	0.075	0.075	3.51	1.90	187	100	[5]
	Ru nanostructures	Al mesh	LAGP	Xe lamp	400 $mA\,g^{-1}$	1000 $mAh\,g^{-1}$	≈2.90	≈3.50	≈83	50	[55]
	Ag nanowires	Carbon cloth	LiTFSI/TEGDME	91.7 $mW\,cm^{-2}$	50 $mA\,g^{-1}$	100 $mAh\,g^{-1}$	2.70	4.11	65.7	40 h	[79]
	Ag nanocubes	Carbon cloth	LiTFSI/TEGDME	UV light	20 $mA\,g^{-1}$	40 $mAh\,g^{-1}$	3.1	3.3	93.9	146 h	[79]
	Ag nanoparticles	Carbon cloth	LiTFSI/TEGDME	/	100 $mA\,g^{-1}$	100 $mAh\,g^{-1}$	3.22	3.25	99	200	[80]
	Ag/Bi_2MoO_6	Carbon cloth	LiTFSI/TEGDME	300 W Xe lamp	50 $mA\,g^{-1}$	0.25 mAh	3.05	3.25	93.8	500 h	[59]
	NiO nanosheets	Ni foam	LiTFSI/TEGDME	300 W Xe lamp	0.01	0.01	2.64	2.73	96.7	60	[81]
Li-CO_2	TiO_2	Carbon cloth	LiTFSI/TEGDME	300 W Xe lamp	0.01	0.01	2.82	2.88	97.9	30	[82]
	RuO_2-TiO_2	Carbon textile	$LiCF_3SO_3$/TEGDME	200 W Xe lamp	250 $mA\,g^{-1}$	1000 $mAh\,g^{-1}$	2.78	2.91	95.5	–	[83]

Table 2: (Continued)

Type	Photocathode Photocatalyst	Current collector	Electrolyte	Light source	Current density [mA cm^{-2}]	Cut-off capacity [mAh cm^{-2}]	Discharge voltage [V]	Charge voltage [V]	Round-trip efficiency 1st [%]	Cycle	Refs.
	TiO_2@Ag	Ti fiber	LiTFSI/$EMIMBF_4$/PVDF-HFP	400 W UV lamp	0.10	0.10	2.49	2.86	86.0	100	[84]
	Cu_2O/CNT	Stainless steel mesh	LiTFSI/TEGDME	500 W Xe lamp	100 mA g^{-1}	100 mAh g^{-1}	≈3.10	≈3.30	≈94	50	[85]
	In_2S_3@CNT/SS	Stainless steel mesh	LiTFSI/TEGDME	/	0.01	0.01	3.14	3.20	98.1	24	[54]
	CNT@C_3N_4	CNT paper	LiTFSI/$EMIMBF_4$/PVDF-HFP	350 W Xe lamp	0.02	0.02	3.24	3.28	98.8	100	[86]
	SiC/RGO	Carbon paper	LiTFSI/TEGDME	500 W Xe lamp	0.01	0.01	2.77	3.24	85.4	50	[87]
	Ru	Carbon nanofiber	LAGP	5–7 kW m^{-2} Xe lamp	500 mA g^{-1}	500 mA g^{-1}	≈2.4	2.99	≈80	450	[88]
	Au@TiO_2	–	LAGP	300 W Xe lamp	0.01	0.01	≈3.1	≈3.5	92.4	–	[89]
Zn-air	α-Fe_2O_3	FTO	KOH/$Zn(Ac)_2$	500 W Xe lamp	0.50	0.17	≈1.15	≈1.64	≈70	75	[51]
	Co_3O_4	ITO	KOH/$Zn(Ac)_2$	AM 1.5	2.00	4.00	≈1.20	≈2.00	≈60	17	[90]
	$NiCo_2S_4$	FTO	KOH/$Zn(Ac)_2$	AM 1.5	2.00	0.67	1.32	1.91	68.8	230	[91]
	$Ni_{12}P_5$@NCNT	Stainless steel mesh	KOH/$Zn(Ac)_2$	300 W Xe lamp	10	–	1.22	1.90	64.2	320	[92]
	$BiVO_4$	FTO	KOH/$Zn(Ac)_2$	500 W Xe lamp	0.50	0.17	≈1.07	≈2.12	51	9	[51]
	ZnO/Cu_2O (ZnO/CuO)	FTO	KOH/$Zn(Ac)_2$	500 W Xe lamp	0.1	–	1.28	1.50	85.3	22 h	[93]
	TiO_2@In_2Se_3@Ag_3PO_4	Carbon paper	KOH/$Zn(Ac)_2$	90 mW cm^{-2} 365 nm UV	0.1	0.1	1.82	0.64	284	210 h	[94]
	C_4N	Carbon paper	KOH/$Zn(Ac)_2$	300 W Xe lamp	0.01	–	–	1.35	–	50	[95]
	C_4N@TiO_2NR	Carbon paper	KOH/$Zn(Ac)_2$	-	0.1	–	0.43	2.02	–	–	[96]
	pTTh	Carbon paper	KOH	50 W LED	0.10	0.24	1.78	≈2.00	≈89	64 h	[97]
	PDTB/TiO_2	Carbon paper	KOH	90 mW cm^{-2} 365 nm UV	–	–	1.90	0.59	322.03	33	[98]
	PEDOTPEO/CNTs/polyurethane	–	PVA/PEO/KOH gel	300 W Xe lamp	1	–	1.00	1.88	53.2	–	[99]
Al-air	CuO/Cu_2O	FTO	NaOH/calcium alginate hydrogel	500 W Xe lamp	1		1.23	–	–	–	[100]
Fe-air	Fe_2O_3	FTO	–	500 W Xe lamp	–	–	–	1.26	–	–	[51]
Zn-CO_2	Cu_2O/CuCoCr-LDH	FTO	KOH/$Zn(Ac)_2$	300 W Xe lamp	0.025	0.0125	1.22	2.07	58.94	55 h	[60]

Defect engineering. Introducing defects into semiconductors can trap charge carriers and inhibit the recombination of photogenerated electron–hole pairs. For example, TiO_2 nanorod arrays were reduced by photoelectrons with increased oxygen vacancies upon illumination.[61] The defect-containing TiO_2 showed improved electron/ion migration and higher catalytic activity than the high-crystalline TiO_2. Another case is that the nitrogen vacancies can extend the absorption edge and enhance the carrier separation of C_3N_4.[86] However, photogenerated electrons and holes can also combine at the defect sites. It is vital to control the defect concentrations rationally.

Heterojunction. A heterojunction is the interface between two semiconductors with different band structures. Rationally combining at least two semiconductors to construct heterojunctions can effectively inhibit recombination and even increase the redox activity of photogenerated carriers.[101,102] Among various heterojunctions, type-II heterojunctions, p–n heterojunctions, direct Z-scheme heterojunctions, and semiconductor–carbon heterojunctions have been proved effective for enhancing electron–hole separation. For the type-II heterojunction, the CB and VB potentials of semiconductor A are higher than those of semiconductor B. Thus, photoelectrons are injected into the CB of semiconductor B, while holes oppositely transfer to the VB of semiconductor A, ensuring effective spatial separation of electron–hole pairs. The p–n heterojunctions further accelerate the electron–hole migration across the interface by building an additional electric field. In the direct Z-scheme heterojunction, the redox potentials of electrons and holes are further optimized for the specific photocatalytic reactions. In the coupled semiconductor–carbon (e.g., graphene, carbon nanotubes) system, the high conductivity of carbon allows the migration of electrons from the semiconductor to the carbon and enhances the carrier separation. Many heterojunctions have been reported for effective carrier separation, such as TiO_2–Fe_2O_3,[62] TiN/TiO_2,[63] Fe_2O_3/C_3N_4,[74] and SiC/graphene.[87]

Schottky junction. The construction of the Schottky junction by combining a semiconductor with a metal, such as gold (Au), silver (Ag), and platinum (Pt) can enhance light absorption and the separation of photogenerated electron–hole pairs. When the work function of the metal is higher than that of the semiconductor, the electrons prefer to flow from the semiconductor to the metal, leading to the formation of the Schottky barrier, which as the energy barrier, prevents the combination of photoelectrons and holes. Besides, some metal nanoparticles can localize the incident light electromagnetic field and generate more carriers. The localized surface plasmon resonances of some specific metals can generate hot electrons, which are injected into the semiconductor. For example, Au nanoparticles were used to extend the absorption of visible light and inhibit the carrier combination of C_3N_4, ensuring efficient utilization of photoexcited carriers in the cathode reactions of a Li–O_2 battery.[58] Various Ag nanostructures also have been widely explored in various light-assisted systems, which will be discussed in Section 3.3.[59,79,80,84]

3.1.4. Introducing External Fields

Introducing external fields (e.g., magnetic field, microwaves, mechanical stress, and temperature gradient) has emerged as a popular strategy to boost photocatalytic efficiencies.[103] This approach can also be transferred to the design of photocathodes. For example, a 3D porous NiO nanosheet/Ni foam photoelectrode was designed to construct a dual magnetic and optical field assisted Li–O_2 battery.[81] At an external magnetic field, the Lorentz force acts oppositely on the photoelectrons and holes, guaranteeing the effective separation of charge carriers. The dual-field-assisted Li–O_2 battery achieved a charge voltage of 2.73 V and a cycling life of 200 h. This strategy provides an environmentally friendly way to enhance battery performance but involves only some specific semiconductor materials.

3.2. Practical Examples of Photocatalysts

3.2.1. Metal Oxides

Among various photocatalysts, TiO_2 has been considered the most promising for academic research and practical applications due to its high photoreactivity, chemical stability, photocorrosion resistance, low cost, and suitable band structure.[104] In 2018, defect-containing TiO_2 nanorod arrays ($\approx$200 nm in diameter, $\approx$1 μm in length) were deposited on a carbon textile through a facile hydrothermal treatment and calcination in air (E_g = 2.98 eV, absorption edge: 416 nm) as the photocathode of a Li–O_2 battery.[61] The photogenerated holes oxidized Li_2O_2 and successfully reduced the charge voltage from 4.31 V to 2.86 V. Long-term illumination introduced more defect sites in TiO_2, and the emerging oxygen vacancies further promoted electron and Li^+ migration, enhancing photocatalytic efficiency and lowering polarizations upon cycling. Based on a seed-assistant growth strategy, TiO_2 on carbon paper as a photocathode was found to promote the OER process in a Zn–air battery.[98] Similarly, TiO_2 nanowires arrays on a carbon cloth were used as the photocathode (E_g = 2.91 eV, absorption edge: 425 nm) for a flexible Li–CO_2 battery which demonstrated a charge voltage of 2.88 V and good cycling stability for 60 h.[82] When a TiO_2 photocathode was integrated into a hybrid Na–O_2 battery with seawater as catholyte, the charge voltage was decreased from $\approx$3.8 to $\approx$2.6 V, corresponding to a round-trip efficiency of $\approx$109 %.[105]

Although TiO_2 has been viewed as one of the most promising photocatalysts, severe carrier recombination of single-component TiO_2 largely impedes its photocatalytic performance. Decorating TiO_2 with other materials is promising to overcome the shortcomings. For example, n-type semiconductor Fe_2O_3 was chosen to tune the electronic behavior of TiO_2 due to its narrow band gap and high chemical stability.[62] The heterostructured TiO_2–Fe_2O_3 photocatalyst exhibited a narrower band gap (1.86 eV, absorption edge: 664 nm) than TiO_2 (2.98 eV, absorption edge: 416 nm) low photoluminescence emission intensity, and high

donor density, indicating broad light absorption and inhibited carrier recombination. A light-assisted Li–O_2 battery showed a narrow polarization gap of 0.19 V and decent cycling stability (Figure 3a). Porous TiN/TiO_2 composite nanowires were also synthesized as light-responsive cathode catalysts for a flexible Li–O_2 battery (Figure 3b).[63] The charge voltage decreased from 3.65 to 2.94 V under illumination, with ≈94 % round-trip efficiency achieved. Besides, Au nanoparticles were deposited onto the surface and inside TiO_2 nanotube arrays as the photocathode of a Li–O_2 battery, which showed much higher discharge capacity in the light than that in the dark (Figure 3c).[64]

Due to its high catalytic activity for decomposing Li_2CO_3, RuO_2 was photodeposited on TiO_2 to serve as the photo-responsive cathode catalyst in a Li–CO_2 battery.[83] The battery presented a quite low charge voltage of 2.91 V under illumination, lower than 3.70 V in the dark. Besides, the RuO_2 surface with its weaker adsorption of Li_2CO_3 is beneficial to the removal of Li_2CO_3 for higher discharge capacity. Ag nanoparticles were used to decorate the TiO_2 nanotube arrays as the photocathode of a Li–CO_2 battery (Figure 3d).[84] The incident light not only excited photoelectrons and holes in TiO_2 but also generated an intensified electric field around the Ag nanoparticles to enable efficient separation and transfer of charge carriers. Benefiting from the synergy of photogenerated carriers and plasmonic interaction, the battery exhibited an ultralow charge voltage

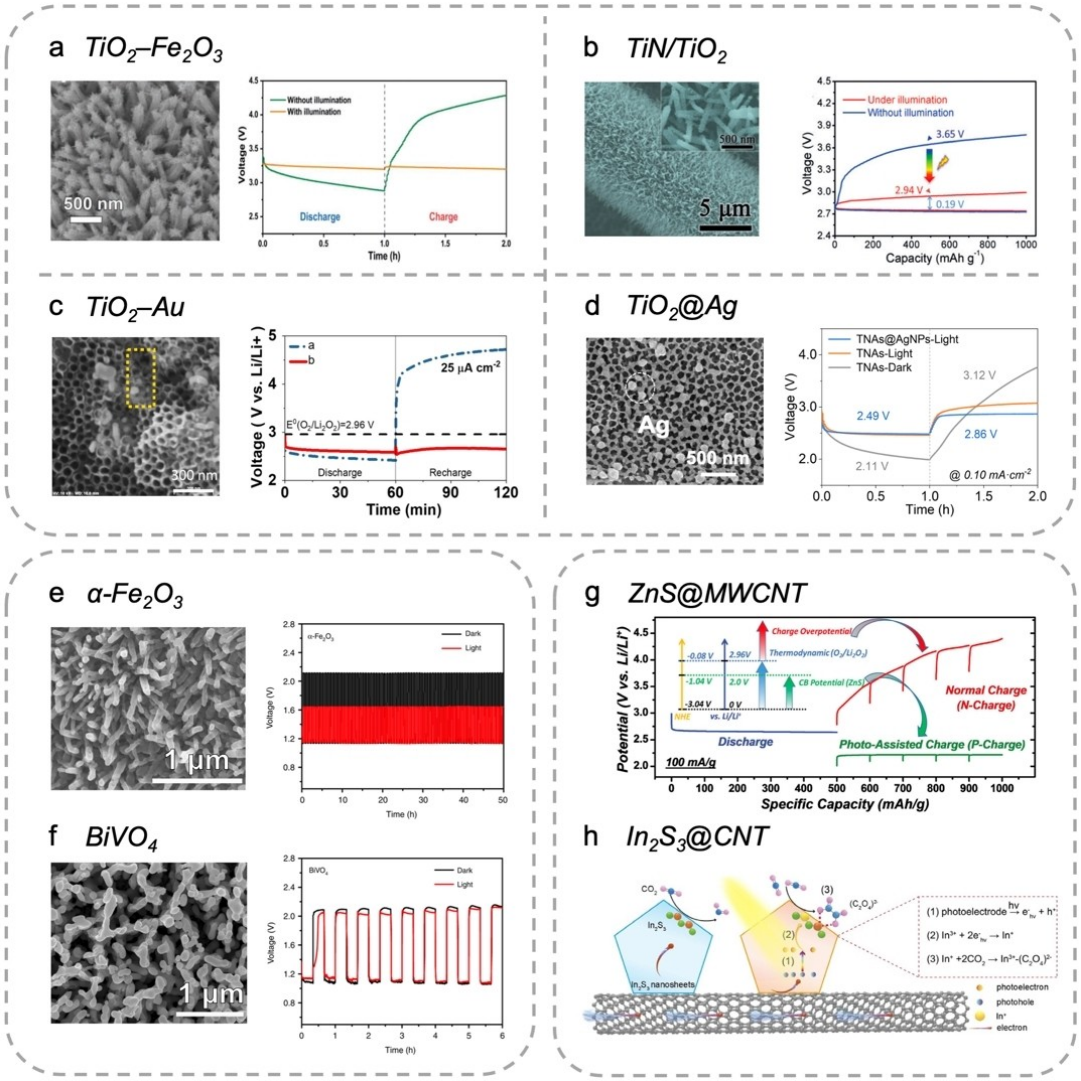

Figure 3. Representative metal-based photocatalysts and their applications in light-assisted metal–air batteries. a–f) Scanning electron microscopy (SEM) images of photocathodes (left) and photo-promoted performances (right). a) TiO_2–Fe_2O_3 hierarchical heterostructured cathode on carbon cloth. Reproduced with permission.[62] Copyright 2020, Wiley-VCH. b) Porous TiN/TiO_2 composite nanowires on carbon cloth. Reproduced with permission.[63] Copyright 2018, Wiley-VCH. c) Carbon- and binder-free TiO_2 nanotube arrays and Au nanoparticles on a Ti mesh. Reproduced with permission.[64] Copyright 2021, Wiley-VCH. d) TiO_2@Ag nanoparticles on a Ti fiber. Reproduced with permission.[64] Copyright 2022, Wiley-VCH. e, f α-Fe_2O_3 and $BiVO_4$ on a FTO glass. Reproduced with permission.[51] Copyright 2019, Macmillan Publishers. g) Galvavanostatic voltage profiles of a Li–O_2 battery containing a ZnS@MWCNT photocathode. Inset, theoretical potential diagram. Reproduced with permission.[68] Copyright 2020, Wiley-VCH. h) Schematic diagram of In_2S_3@CNT photocathodes. Reproduced with permission.[54] Copyright 2020, Wiley-VCH.

of 2.86 V at 0.10 mA cm^{-2} and good cycling stability with 86.9 % round-trip efficiency after 100 cycles.

TiO_2 can only utilize the limited ultraviolet light of the solar spectrum due to its wide forbidden band. This has prompted scientists to explore other inorganic semiconductor materials for efficient visible-light utilization. Distinct from TiO_2, WO_3 demonstrates a decent visible-light response (E_g = 2.5–2.8 eV), good electron mobility, and hole diffusion length. In 2019, binder-free WO_3 nanowires were deposited on a carbon textile as the photocathode for a Li–O_2 battery, which showed a discharge/charge voltage of 2.71/3.63 V at the 1st cycle and 2.89/3.55 V at the 100th cycle at 0.06 mA cm^{-2} under visible light.[65] To inhibit recombination of photoelectrons/holes inside WO_3, the same group further decorated WO_3 with carbon nitride as photocathode of a Li–O_2 battery, which demonstrated a lower charge voltage of 3.69 V than that of WO_3 (3.99 V) at 0.10 mA cm^{-2} under visible-light irradiation.[106] Compared with TiO_2, WO_3 shows better visible-light response and chemical stability but inferior OER activity.

With high photoelectrochemical/chemical stability and suitable band gap (E_g = 1.9–2.2 eV), α-Fe_2O_3 has also been applied in metal–air batteries with alkaline electrolytes. In 2019, a light-assisted Zn–air battery was constructed based on an α-Fe_2O_3 photocathode, which delivered charge and discharge voltages of 1.64 and 1.15 V for 50 h in light, corresponding to a round-trip efficiency of 70.3 % (Figure 3e).[51] In contrast, only 54.5 % efficiency was achieved in the dark. The authors identified, the limiting factor for long-term stability as the passivation of Zn anode in alkaline electrolyte rather than the erosion of α-Fe_2O_3. Besides, they also fabricated a Fe–air battery based on an α-Fe_2O_3 photocathode with a charge voltage of 1.26 V in the sunlight. Inspired by this study, α-Fe_2O_3 nanorods were used to catalyze the cathode reactions of a hybrid Li–O_2 battery ($O_2 + 4Li + 2H_2O \leftrightarrow 4LiOH$).[52] O_2 was reduced to soluble OH^- in the electrolyte instead of solid products during discharging; in the charge process, photogenerated holes oxidized OH^- to release O_2. Benefiting from the superior catalytic performance and photoelectrochemical stability of α-Fe_2O_3, the resulting battery delivered discharge and charge voltages of 2.56 V and 3.15 V. To overcome the poor electron-transfer and severe carrier recombination of α-Fe_2O_3, the same group further coated α-Fe_2O_3 nanorods array with NiOOH for a hybrid Li–O_2 battery.[66] The holes at NiOOH firstly oxidized Ni^{II} to Ni^{III} and then participated in the OER to improve the current density. Finally, a charge voltage of 3.03 V and a high round-trip efficiency of 88 % was achieved. The above examples proved that α-Fe_2O_3 can improve OER kinetics in different prototypes of metal–air batteries, and the catalytic performance can be further improved by combining with second components.

Copper (Cu) oxides are also used as photocatalysts for light-assisted metal–air batteries. For example, Cu_2O can effectively promote Li_2CO_3 decomposition in the charge stage of the Li–CO_2 battery.[85] The valence change of Cu (Cu_2O/CuO) was considered as a key factor for achieving high efficiency in a Zn–air battery.[93] CuO and Cu_2O were also used to promote ORR process of an Al–air battery.[100] A Cu_2O/CuCoCr-layered double hydroxide with ultrathin p-n type heterojunction nanosheets was designed for a Zn–CO_2 battery. The heterostructure photocatalyst was beneficial to converting CO_2 to CO during discharging and water oxidation during charging.[60] Most reported metal oxides are n-type semiconductors which mainly enhance the OER process during charging but show limited effects on the ORR process during discharging. To this end, the p-type semiconductor lanthanum ferrite ($LaFeO_3$) was coated on an FTO glass as the photocathode of a hybrid Li–O_2 battery.[67] With a VB position more positive than the E_{O_2/H_2O} (1.23 V vs. RHE), photoelectrons of $LaFeO_3$ can reduce O_2 to OH^- with an increased discharge voltage from 2.81 to 3.24 V. $LaFeO_3$ also presents decent stability in electrolytes but limited effects on the charging process.

3.2.2. Metal Sulfides

Besides metal oxides, metal sulfides have also been used in light-assisted metal–air batteries owing to their suitable band structure and electrochemical/chemical stability. Owing to its special conduction band potential (2.0 V vs. Li^+/Li), zinc sulfide (ZnS) was chosen to decompose Li_2O_2. In 2017, ZnS was coated onto multiwalled carbon nanotubes (ZnS@MWCNT) as the photocathode in Li–O_2 battery, which decreased the charge voltage to 2.2 V in the light (Figure 3g).[68] The same group further used ZnS@CNT as a photoelectrode coupled with an Li_xSi alloy anode and a plastic crystal solid electrolyte in an all-solid-state Li-ion O_2 battery .[53] The photocathode enabled an ultralow charge voltage of 2.08 V at the first cycle and remained at ≈2.2 V after 50 cycles, much lower than the theoretical equilibrium voltage of 2.86 V. Besides, cadmium selenide/ZnS quantum dots with CNT (CdSe/ZnS QD@CNT) and MoS_2/$ZnIn_2S_4$ were synthesized to decrease the overpotential of Li–O_2 batteries under light.[69,70]

Later in 2020, In_2S_3 nanosheets were uniformly coated on CNT networks to provide abundant active sites for redox reactions and a shorter diffusion length for photogenerated carriers.[54] Because the CB level of In_2S_3 (3.38 eV) is lower than the work function of CNT (4.90 eV), photoelectrons in the CB level of In_2S_3 can spontaneously flow into CNT at the interface and enhance carrier separation. The photocathode produced a higher photocurrent response, weaker photoluminescence, and higher activity for CO_2RR and CO_2ER than In_2S_3 without CNT. The hierarchical porous In_2S_3/CNT photoelectrode was integrated into a light-assisted Li–CO_2 battery, which achieved a high discharge voltage of 3.14 V surpassing the thermodynamic limit of 2.80 V and ultralow charge voltage of 3.20 V, corresponding to a round-trip efficiency of 98.1 % (Figure 3h). The authors further proposed that the reduction of In^{3+} to In^+ in the photocatalyst under illumination serves to pre-activate CO_2. Besides, $NiCo_2S_4$ was used to boost ORR and OER processes in an alkaline Zn–air battery.[91]

3.2.3. Other Metal-Based Semiconductors

Metal vanadates have also been used at the photocathodes. $BiVO_4$ has been explored as the photocatalyst in an aqueous Zn–air battery and a hybrid Li–O_2 battery.[51,55] $BiVO_4$ demonstrated faster charge transfer and higher response current but inferior stability and rapid deactivation due to the severe photocorrosion and higher solubility in the alkaline electrolyte compared to α-Fe_2O_3 (Figure 3f). Recently, $CeVO_4$ was synthesized for a light-assisted Li–O_2 battery,[71] which achieved a low charge voltage of 3.48 V and discharge capacity of 6.14 mAh cm^{-2}. Besides the superior photoelectrochemical property, $CeVO_4$ also demonstrated superior O_2 adsorption and efficient conversion ability of superoxide species to Li_2O_2, avoiding the decomposition of electrolyte and cathode during discharging.

The hybrid perovskites were also assembled onto carbon materials as photoelectrodes in Li–O_2 batteries recently.[78] The good intrinsic stability of the perovskite cathode and the enhanced charge transfer at the perovskite/carbon interface contributed to the final superior performance. Besides, a stable iron-based metal–organic framework was used to encapsulate $CsPbBr_3$ nanocrystals as synergistic photocathode materials for a light-assisted Li–O_2 battery, in which $CsPbBr_3$ and the metal–organic framework acted as optical antennas and ORR/OER catalytic sites, respectively.[77] The composite photocathodes enabled lower overpotentials and longer lifespans than the batteries based on either single-component photocatalyst.

3.2.4. Carbon Nitrides

Restrained by the wide band gap of above 3.0 eV, most metal-based photocatalysts can only harvest ultraviolet light accounting for ca. 7 % of the solar spectrum. The development of visible-light-responsive photocatalysts is being continuously pursued. The family of two-dimensional polymeric carbon nitrides with varying stoichiometry (C_xN_y) has attracted extensive attention owing to their facile synthesis, tunable structures, unique physicochemical properties, and wide applications. Polymeric carbon nitrides (C_3N_4) attract the most attention due to their intriguing electronic structure and excellent chemical stability,[107] and they have been implemented in significant applications in photocatalysis,[108] electrocatalysis,[109] and energy storage.[110–112]

In 2014, C_3N_4 was first integrated into a rechargeable Li–O_2 battery with I^-/I_3^- redox mediators.[56] During charging in the light, I^- ions were oxidized to I_3^- ions by the holes, and then I_3^- ions diffused to oxidize Li_2O_2 to O_2 at the cathode surface and were reduced back to complete a full redox cycle. The battery achieved an ultralow charge voltage of 1.9 V under illumination compared with 3.55 V in the dark, and a discharge voltage of ≈2.7 V, leading to 142 % round-trip efficiency. The redox mediators play a critical role in reducing the charge overpotentials, but I_3^- ions would inevitably migrate across to the Li anode and form a non-conductive LiI layer, which would reduce the utilization of I_3^- and increase the internal resistance of the battery. In 2016, the group further reported a C_3N_4-based Li–O_2 battery without redox mediators,[57] which achieved a comparable low charge voltage of 1.96 V and a lifespan of 70 cycles under illumination. The holes directly oxidized Li_2O_2 to O_2 and Li^+, while photoelectrons were injected into the carbon paper and migrated to the anode to reduce Li^+ to Li. Similarly, the metal-free photocatalysts only demonstrated catalytic effects for OER. In 2019, C_3N_4 was used as a bifunctional photocatalyst to simultaneously boost the discharge and charge kinetics of a Li–O_2 battery (Figure 4a).[72] The battery achieved a discharge voltage of 3.22 V and a charge voltage of 3.38 V at 0.04 mA cm^{-2}, leading to a round-trip efficiency of 95.3 %. Raman analysis revealed that O_2 was first reduced to O_2^- and then O_2^{2-} by photoelectrons in the CB of C_3N_4, and evolved into the final product Li_2O_2; in a reverse charge, the solid products were decomposed by the holes in the VB of C_3N_4 at a plus voltage. The above results can be related to the diverse structures and properties of carbon nitrides synthesized in different ways.

In order to further promote the battery performance, researchers decorated C_3N_4 with various second components. Defect-containing C_3N_4 decorated with Au nanoparticles (Au/N_V-C_3N_4) was designed as the photocathode to promote the cathode reactions of a Li–O_2 battery (Figure 4b).[58] The weaker photoluminescence emission intensity, more prolonged carrier lifetimes, and stronger surface photovoltage signal of Au/N_V-C_3N_4 relative to those of N_V-C_3N_4 revealed the efficient separation and high carrier concentration. During discharging, O_2 was preferentially adsorbed on nitrogen vacancies of N_V-C_3N_4 and reduced to Li_2O_2 by photogenerated hot electrons from plasmonic Au nanoparticles. Reversely, Li_2O_2 was decomposed by the holes on Au nanoparticles plus an applied voltage during charging. The battery delivered a discharge/charge voltage of 3.16/3.26 V at 0.05 mA cm^{-2} under illumination, corresponding to a round-trip efficiency of 97.0 %. The researchers further designed a step-scheme junction comprising Fe_2O_3 and C_3N_4 of which the internal electric field and interfacial Fe–N bonds can effectively promote the separation and migration of charge carriers (Figure 4c). The photoelectrons from C_3N_4 and holes from Fe_2O_3 can accelerate the discharge and charge reactions, generating a high discharge voltage of 3.13 V and a charge voltage of 3.19 V in the light.[74] Recently, our group utilized a heterostructure photocathode comprising interwoven CNT scaffolds and defect-containing C_3N_4 coatings to enhance the performance of a Li–CO_2 battery. The favorable charge transfer between C_3N_4 and CNT ensured the efficient separation of excited photoelectrons and holes and effective photoenergy utilization for reaction kinetics. The Li–CO_2 battery showed an ultralow voltage hysteresis of 0.04 V, corresponding to a round-trip efficiency of 98.8 %.

Different from C_3N_4, the n-type semiconductor C_4N displays a narrow band gap (1.99 eV), strong photocurrent response, and superior bifunctional reactivity (Figure 4d).[95] Theoretical calculations indicate that the bifunctional ORR/OER activities are associated with two separate active sites

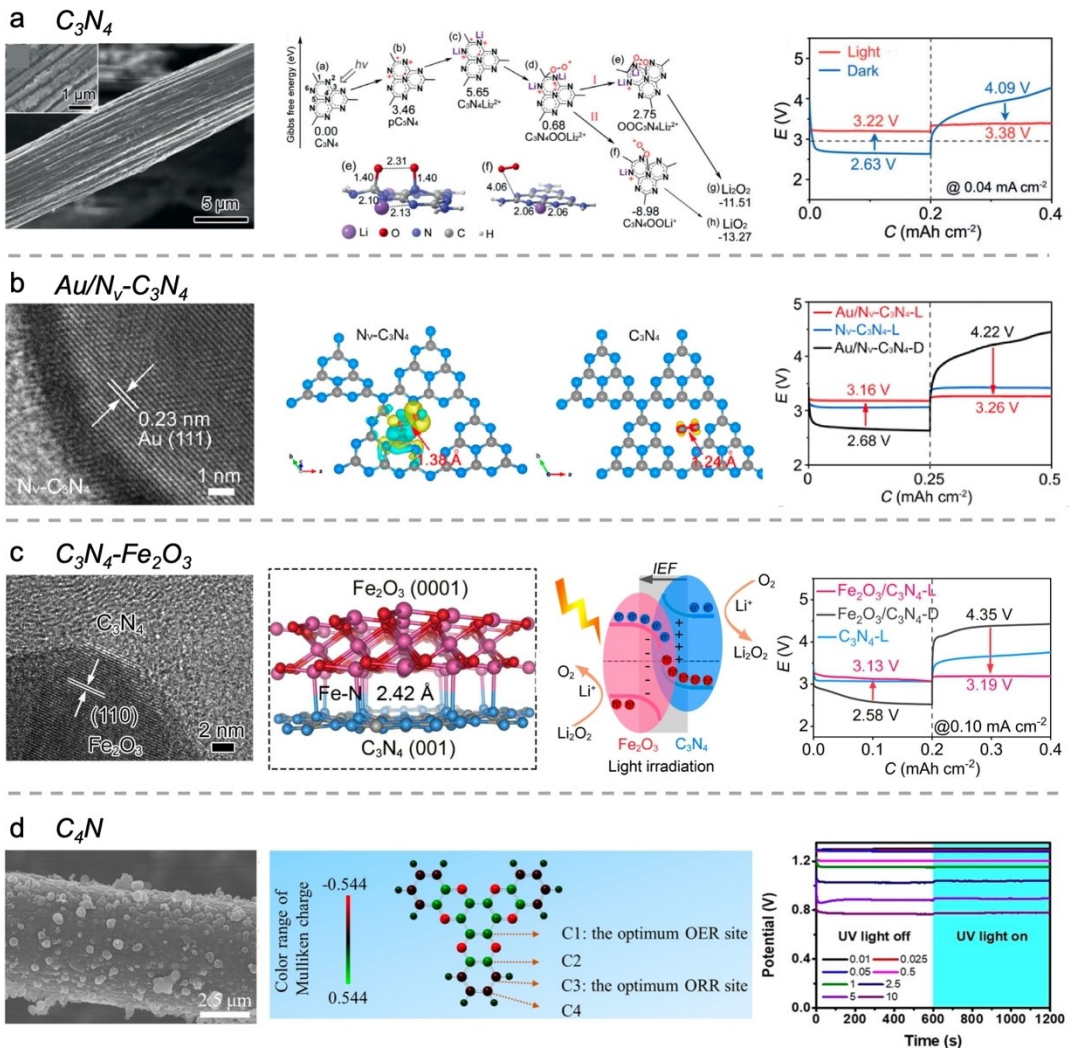

Figure 4. Representative carbon nitride photocatalysts and their applications in light-assisted metal–air batteries. a–d) Scanning electron microscopy and transmission electron microscopy (TEM) images of photocatalysts (left), molecular or band structure (middle), and photo-promoted performances for a–c) Li–O_2 batteries and d) Zn–air battery. a) C_3N_4 on carbon paper. Reproduced with permission.[72] Copyright 2019, Wiley-VCH. b) Au nanoparticle-decorated C_3N_4 with nitrogen vacancies. Reproduced with permission.[58] Copyright 2021, National Academy of Sciences. c) Step-scheme junction with hematite on carbon nitride.[74] Copyright 2022, Wiley-VCH. d) Mesoporous C_4N particles on carbon paper. Reproduced with permission.[95] Copyright 2021, Wiley-VCH.

of C_4N. The C_4N-enabled Zn–air battery delivered a good rate capability (operating at 10 mA cm^{-2}) under UV light, an ultralow charge voltage of 1.35 V under visible light, and a round-trip efficiency of 97.78 %. The same group further designed a step-scheme heterostructure comprising C_4N and TiO_2 nanorods as the photoelectrode of a Zn–air battery. The staggered band arrangement induces an S-type charge migration via a strong internal electric field, ensuring increased redox ability and efficient spatial separation of photogenerated carriers. Combining this photoelectrode with an asymmetric acid–base electrolyte, a unique integrated system was constructed that can utilize light and chemical neutralization energy to mediate battery performance.[96]

3.2.5. Polymers

Many metal-based semiconductors and carbon nitrides demonstrated limited effects on the discharge processes (ORR or CO_2RR) of metal–air batteries. Polymer semiconductors have been widely used in photocatalytic ORR owing to their facile synthesis, low cost, wide light absorption, and tunable band structure. Notably, polythiophene (pTTh), a p-type polymeric semiconductor, has been identified as an effective photocatalyst to promote the ORR process of a glucose–air biofuel cell[113] and a H_2–O_2 fuel cell.[114] Inspired by these studies, pTTh was used to accelerate the ORR of a Zn–air battery in 2019.[97] The pTTh electrodeposited on carbon paper presented a hierarchical spherical structure (4–5 μm in diameter) assembled from nanosheets (20–50 nm in thickness) (Figure 5a). Under illumination, photoelectrons in the CB of pTTh were

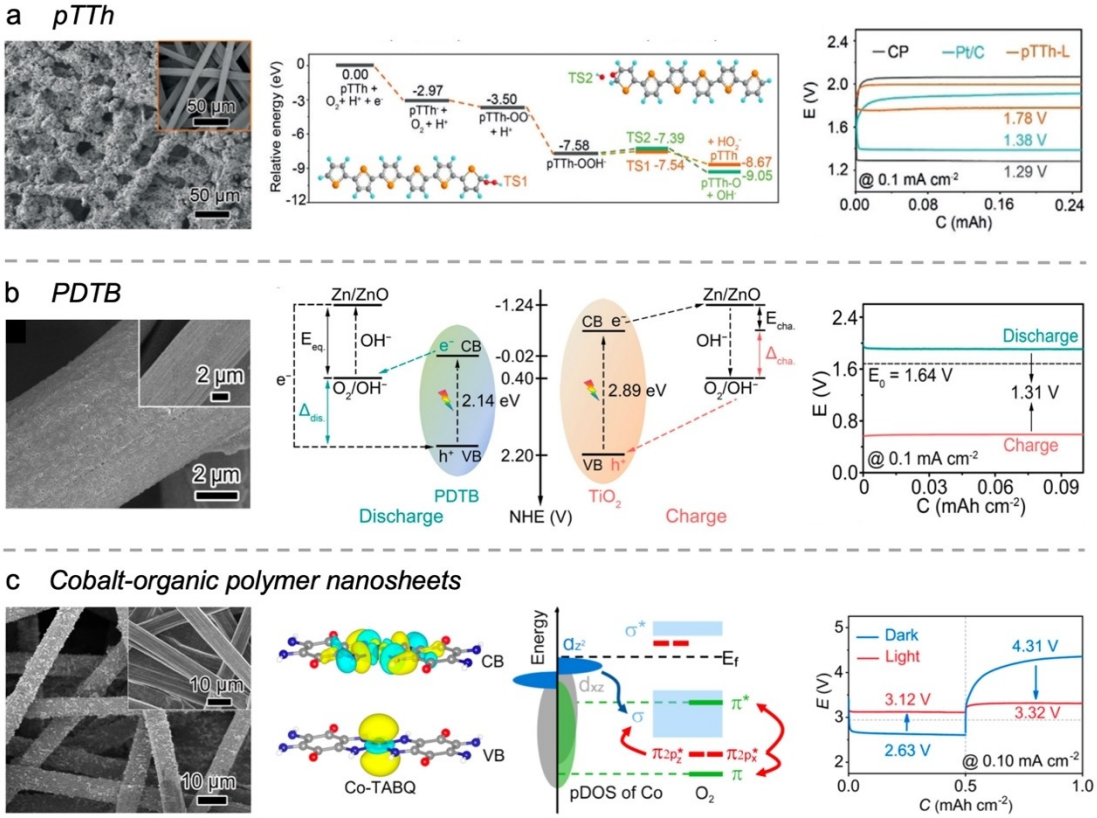

Figure 5. Representative polymer photocatalysts and their applications in the light-assisted metal–air batteries. a–c) Scanning electron microscopy images of photocathodes (left), the working mechanism (middle), and photo-promoted performances (right). a) pTTh for Zn-air batteries. Reproduced with permission.[97] Copyright 2019, Wiley-VCH. b) PDTB for Zn-air batteries. Reproduced with permission.[98] Copyright 2020, Wiley-VCH. c) Cobalt-organic polymers for Li-O_2 batteries. Reproduced with permission.[75] Copyright 2020, American Chemical Society.

harvested by O_2 to generate HO_2^- which then disproportionated to stable OH^-. Meanwhile, the holes drove the oxidation of Zn to ZnO at the anode via the external circuit. The battery achieved an output voltage of 1.78 V under irradiation, surpassing the thermodynamic limit of 1.64 V. Researchers also explored some interesting applications beyond the light-assisted Zn–air battery, such as an integrated electricity/H_2O_2 cogeneration and waste treatment system[115] and a self-powered sensing platform.[116] Recently, pTTh coupled with I_3^-/I^- as redox mediators was used to reduce the overpotentials of a Li–O_2 battery.[76] Photoelectrons contributed to the ORR process, while holes oxidized I^- to I_3^- and decomposed Li_2O_2, resulting in a lowered charge voltage of 3.19 V.

To accelerate the discharge and charge reactions simultaneously, a photo-enhanced Zn–air battery was constructed with poly(1,4-di(2-thienyl)benzene (PDTB) and TiO_2 as photocathodes (Figure 5b).[98] During discharging, PDTB was excited for ORR, with photoelectrons transferring to reduce O_2 and holes migrating to oxidize Zn to ZnO via the external circuit. In the charging process, TiO_2 produced holes to drive the sluggish OER. The battery delivered a high discharge voltage of 1.90 V and a low charge voltage of 0.59 V. With a tunable band structure and well-dispersed single metal sites, metal–organic polymers have emerged as promising materials for electrocatalytic and photocatalytic applications. Recently, metal–organic polymer nanosheets composed of cobalt-tetramino-benzoquinone (Co-TABQ) were synthesized with an absorption edge at 585 nm and used to reduce the overpotentials of a Li–O_2 battery under visible light (Figure 5c).[75] Upon discharge, O_2 was first adsorbed on the Co atoms of Co-TABQ and accepted electrons from Co atoms for its reduction to LiO_2 and transformation into the final product, Li_2O_2. The holes of Co accelerated the fast decomposition of Li_2O_2 to O_2 and Li^+ with the aid of an applied voltage in the charging process. The battery demonstrated discharge and charge voltages of 3.12 and 3.32 V, respectively, corresponding to a round-trip efficiency of 94.0 %.

3.2.6. Si-Based Semiconductors

Besides the above typical photocatalysts, Si-based semiconductors also have been explored in light-assisted metal–air batteries. In 2021, a kind of novel ultralarge (≈63 μm) and few-layer (≈3 layers) siloxane nanosheet material was synthesized with superior light harvesting and inhibited carrier recombination,[5] which achieved a discharge voltage of 3.51 V and a charge voltage of 1.90 V in a light-assisted Li–O_2 battery, corresponding to a round-trip efficiency of up to 185 %. The battery also demonstrated an impressive rate

performance (129 % efficiency at 1 mA cm^{-2}) and superior durability (92 % efficiency retention after 100 cycles). In addition, a light-assisted Li–CO_2 battery was designed with SiC grown on reduced graphene oxide as the photo-electrocatalytic hybrid cathode.[87] As a conductive matrix, graphene could effectively separate and transfer photoelectrons concentrated on the SiC and prevent unfavorable carrier recombination. Benefitting from the superior light absorption property of graphene, the SiC/graphene composites showed enhanced visible light absorption (bandgap: 2.29 eV) than pure SiC (bandgap: 2.63 eV). The initial discharge/charge voltage of 2.55/4.17 V in the dark significantly increased/decreased to 2.77/3.28 V in the light, indicating the enhanced kinetics under illumination. The battery delivered a lower overpotential of 0.42 V in light compared with 1.54 V in the dark and an energy efficiency of 84.4 % (not considering solar energy).

3.3. Photothermal Materials

Besides semiconductor photoelectric materials, photothermal materials have also been introduced to the air cathodes of metal–air batteries, which can convert light energy into heat to promote sluggish ORR/OER and CO_2RR/CO_2ER kinetics. In 2020, an ultralow-temperature all-solid-state Li–air battery was constructed based on a plasmon-enhanced photothermal air electrode comprising close-packed Ru nanoparticles (5–20 nm) and CNT (Figures 6a, b).[55] The engineered black plasmonic cathode efficiently harvested light energy from the ultraviolet to the near-infrared range and converted light to heat. The temperature of the cathode surface reached ≈70 °C under illumination, even in a cryogenic environment of −73 °C. The battery displayed a lifetime of 15 cycles and a high discharge capacity of 3600 mAh g^{-1} at −73 °C (Figure 6c). Plasmonic Ru catalysts are also beneficial to C–O bond cleavage during discharging and CO_2 evolution during charging of Li–CO_2 batteries; this is attributed to the energetic hot carriers produced by nonradiative decay of localized surface plasmons.[88] Besides, a wide-temperature all-solid-state Li–air battery was demonstrated that could operate from −73 to 120 °C; the key to this battery was the plasmonic photothermal cathode composed of ruthenium oxide nanoparticles assembled on carbon nanotubes (Figure 6d).[117] The cathode captured a broad solar spectrum from 200 to 2500 nm and converted it to heat for warming up the battery while stabilizing the substantial charge carrier concentration caused by oxygen vacancies. The illumination induced a temperature increase for the cathode from −73 to 20 °C within 400 s (Figure 6e). Benefitting from the enhanced charge transfer and storage at high temperatures, the battery demonstrated high discharge capacity and a stable cycle from −73 to 120 °C. Hemoglobin-like (or doughnut-shaped) products (1–3 nm in diameter) were obtained at −73 °C, and a dense Li_2O_2 layer consisted of rugby-like (or football-shaped) product particles (8–18 nm in diameter) at 120 °C, demonstrating the effect of temperature on product nucleation and growth (Figure 6f).[118,119]

Recently, plasmonic Ag nanoparticles were proved to simultaneously induce the photothermal heating of the cathode and hot-electron effects caused by local surface plasmon resonance.[79,80] Both of the effects contributed to the ORR/OER kinetics of a Li–O_2 battery; significantly, the respective contribution of each effect to the performance enhancement was identified. By comparison, Ag nano-

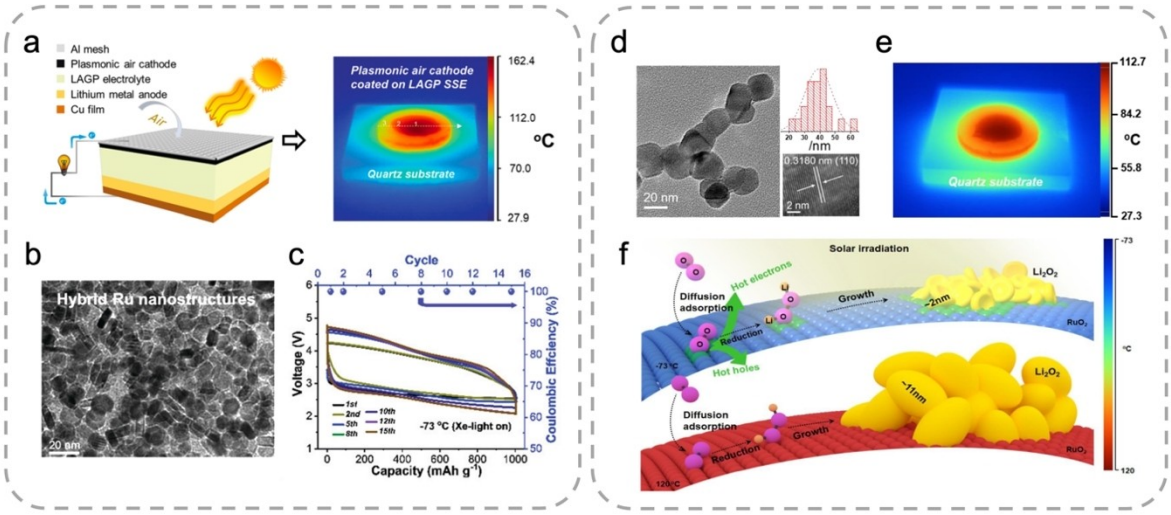

Figure 6. Representative photothermal cathodes and their applications in light-assisted Li–air batteries. a) Schematic diagram of a photothermal all-solid-state Li–air battery with the black air cathode anchored on the LAGP electrolyte and an IR image of the plasmonic air cathode under Xe-lamp irradiation. b) Transmission electron microscopy image of single-layer plasmonic Ru nanoparticles. c) Electrochemical performance at ultralow temperatures. Reproduced with permission.[55] Copyright 2020, Royal Society of Chemistry. d) Transmission electron microscopy image of RuO_2 nanoparticles (inset: histogram of size distribution and a high-resolution image). e) IR image of a RuO_2-based photothermal cathode under solar irradiation. f) Schematic illustrating the influence of temperature on the formation of discharge products. Reproduced with permission.[117] Copyright 2021, Elsevier.

particles produced lower temperature enhancement than Ru-based counterparts. The same group designed an Ag/Bi_2MoO_6 hybrid cathode with broad light absorption and superior electrochemical activity for O_2 reduction/evolution.[59] Photoelectrons from Ag nanoplates based on the localized surface plasmon resonance can be injected into the oxygen vacancies of Bi_2MoO_6 and promote the ORR kinetics. Similarly, the effects of Au nanoparticles in a Li–CO_2 battery also have been confirmed.[89]

Besides metal-based nanoparticles, carbon materials also showed potential as photothermal cathodes. Based on a multiscale conjugated block-copolymer-CNT-polyurethane foam as an air electrode, a multisensing smart rechargeable Zn–air battery was proposed.[99] Upon irradiation, the battery temperature rapidly increased from ≈18 to ≈53 °C within 90 s, which led to an increased discharge voltage (0.92–1.00 V) and a lowered charge voltage (1.96–1.88 V), corresponding to the rise in round-trip efficiency (46.9 %–53.2 %). Similarly, a hydrophobic black carbon fiber cloth was used as the photothermal-responsive, waterproof, and breathable layer that could convert the most absorbed photoenergy into heat to raise the temperature of a Zn–air battery.[120] Under visible-light illumination (300 mW cm^{-2}), the battery temperature was enhanced up to 73.1 °C, resulting in accelerated ion/electron transfer and boosted ORR kinetics. The discharge voltage rose from 0.85 V in the dark to 1.02 V under illumination, with a 20 % increase in energy output.

4. Influence of Light on the Battery

Light is like a double-edged sword for the battery. As discussed above, light can accelerate cathode kinetics, enhance thermodynamic reversibility, and boost the electrochemical performances of metal–air batteries with the assistance of reactive photoelectrons and holes. Particularly, light can mediate reaction pathways in a thermodynamically favorable way and influences the growth of discharge products in aprotic Li–O_2 (CO_2) batteries. However, light also poses inevitable threats to battery stability, such as photocorrosion of photocatalysts and electrolyte decomposition. Current research mainly focuses on the design of photocathodes facing illumination, while some studies have been devoted to enhancing the electrolytes in these special battery systems. In comparison, no studies regarding metal anodes in light-assisted batteries have been reported. In this section, the effects of light on metal–air batteries will be systematically discussed in terms of the photocathode and the electrolyte.

4.1. Photocathode

4.1.1. Influencing Discharge Product Growth

As is known, the discharge products Li_2O_2 (Li_2CO_3 + C) for non-aqueous Li–O_2 (CO_2) batteries can exhibit different morphologies or structures (sizes, shapes, and crystalline) at various potentials,[121–123] electrolytes,[124–126] electrocatalysts,[17,127] and temperatures.[118,128] The structure of the products will significantly influence the subsequent charging process and also the thermodynamic reversibility of battery.[62,129–133] Generally, it is believed that film-shaped products formed via a surface growth pathway can lower charge overpotentials due to the enhanced electron transfer between insulated products and the cathode surface. Still, it can also prevent mass transport and limit achievable capacity. In comparison, particle-shaped solid products grown via a surface pathway tolerate high discharge capacity due to more exposed active area. Typically, the discharge products with terrible crystalline or amorphous structures are readily decompose during charging.

Recently, researchers observed that the discharge products exhibit different morphologies under illumination and dark. They have proposed some possible mechanisms for these structural differences and speculated that these differences would further influence the subsequent decomposition during charging. For example, layered toroidal products were deposited at the TiO_2–Fe_2O_3 photoelectrode surface in the dark, while film-like products formed among TiO_2 arrays under illumination in a Li–O_2 battery (Figure 7a, b).[62] They pointed out that the photocathode under illumination with abundant photoelectrons was more favorable for O_2 adsorption and mass transfer than in in the dark, thus resulting in different product growth pathways and final morphologies (Figure 7c). The light-mediated film-shaped products favored mass transport and electron transfer to ensure fast charge kinetics. A similar phenomenon was also observed at the TiO_2 cathode in the Li–CO_2 battery.[82] Bulk products were deposited on the surface of the In_2S_3@CNT in the dark, in comparison with film-shaped products in the light (Figure 7d, e).[54] The authors explained that the enriched photoelectrons at the cathode could adsorb CO_2 and Li^+, providing more nucleation sites to generate film-shaped products (Figure 7f). Different from the above results, the same group also noticed that tabular products were erected on SiC sheets under illumination, compared with large-area film-like products in the dark.[87]

The above differences can be related to the distribution of the photocatalysts in the photocathodes. For the In_2S_3@CNT cathode, In_2S_3 nanosheets are evenly distributed at the cathode and provide numerous nucleation sites for the generation of film-like products, while the isolated SiC sheets at the photocathode result in the formation of discrete products. Recently, our group also discovered that the discharge products presented similar spherical shapes on the CNT@C_3N_4 cathode in a Li–CO_2 battery, but the product particles in the light were much smaller than those in the dark. The light-induced small product particles can be easier to decompose than those in the dark.[86]

The nucleation and growth of discharge products in practical metal–air batteries is pretty complex and related to the battery materials/configurations, testing methods, and environmental conditions. Generally, amorphous products with good ion and electron transfer are considered easier to decompose than the discharge products with good crystallinity and large size. In the above studies, some possible

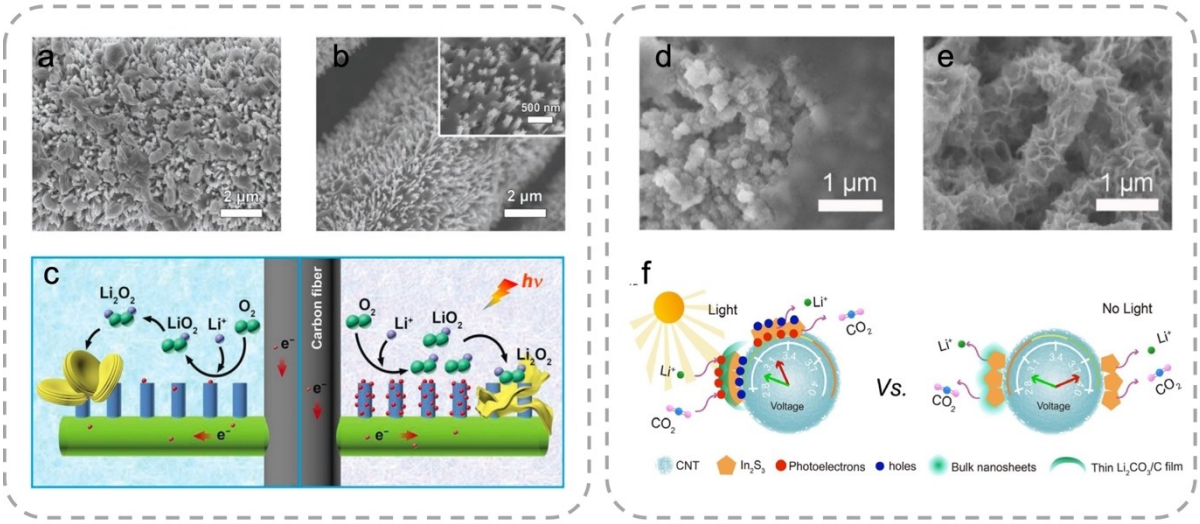

Figure 7. Influence of light on the formation and decomposition of discharge products in the aprotic Li–O_2 (CO_2) batteries. a, b) Scanning electron microscopy images of TiO_2/Fe_2O_3 cathodes after first discharge a) without and b) with illumination. c) Schematic illustration of discharge mechanisms with and without illumination. The toroidal-like products are deposited on the top of the catalyst arrays without illumination, while the film-like Li_2O_2 is generated among the catalyst arrays with illumination. Reproduced with permission.[62] Copyright 2020, Wiley-VCH. d, e) Scanning electron microscopy images of In_2S_3/CNT cathodes after discharging d) in the light and e) dark. f) Schematic diagram of product formation pathways in the light and dark. Reproduced with permission.[54] Copyright 2020, Wiley-VCH.

growth pathways were proposed based on ex situ results but lacking in-depth research tools. Future studies can utilize more advanced characterization and simulation tools to analyze the influence of the photocatalytic process on product formation/decomposition. Specifically, the contribution of heat under illumination should be excluded when studying the effects of the photocatalytic process.

4.1.2. Mediating the Thermodynamic Pathway

The cathode reactions could progress in a thermodynamically favorable pathway under illumination. For example, Co-TABQ was used as a photocatalyst in a Li–O_2 battery.[75] Density functional theory revealed the photogenerated electrons in the CB are transferred from Co atoms to O_2, leading to activation of the adsorbed O_2 and the generation of Li_2O_2 during discharging. Li_2O_2 formation is thermodynamically favorable due to the downhill free energy under illumination. In comparison, the adsorption and activation of O_2 on the photocathode is thermodynamically unfavorable, with increased free energy. A photo-induced reaction process was discovered in a Li–CO_2 battery with In_2S_3@CNT/SS as the photocathode.[54] CO_2 was adsorbed on the cathode surface and reduced with the aid of In^+. The outer electrons of In^+ can transfer to a strong electron acceptor (i.e., O in CO_2 reduction products) to form an In^{3+}-$C_2O_4^{2-}$ adduct via an In–O bond. The intermediate step benefits the discharging process under light, referred to as "pre-activating" CO_2 through adduct formation.

4.1.3. Photocorrosion

The photoelectrochemical stability of photocatalysts is also considered a key influential factor for battery life. Photocorrosion refers to the increase in photogenerated charge carriers participating in the self-oxidation and reduction of semiconductors instead of the target reactions, such as water splitting.[134] For example, $BiVO_4$ experienced intensive photocorrosion in a basic electrolyte under illumination, with an 84.6 % decrease in the photocurrent intensity within several minutes.[51] X-ray diffraction patterns revealed the remarkably decreased peak intensity, and scanning electron microscopy images showed the dissolution of $BiVO_4$. Correspondingly, the Zn–air battery with a $BiVO_4$ photoelectrode exhibited poor cycling stability although the battery exhibited an ultralow charge voltage at the initial stage.[51] In comparison, Fe_2O_3 exhibited high photocorrosion resistance and was considered a better choice for an aqueous Zn–air battery with an alkaline electrolyte. Toward the long-term practical application of batteries, more research efforts should be devoted to developing more stable semiconductor photocatalysts in practical electrolytes and operating conditions for more stable metal–air batteries. For example, photocathode stability can be enhanced by introducing a protection layer to pristine materials. As a demonstration, pTTh was deposited on the Cu_2O surface to inhibit photocorrosion and promote photoresponse.[135] In addition to the photocathode, the stability of metal anodes also needs to be emphasized to achieve metal–air batteries with long durability.[136]

4.2. Electrolyte

The electrolyte is essential for metal–air batteries; it coordinates mass transport in the whole battery system, stabilizes reaction intermediates, sometimes determines reaction pathways, and directly influences battery performance.[7,137–139] As known, large overpotentials will trigger parasitic reactions in the electrolyte and shorten the life span of the battery; thus, optimized electrolytes are constantly explored.[140–143] Although light-assistance can effectively reduce the discharge/charge overpotentials in batteries, long-term illumination also poses an inevitable threat to electrolyte stability. For one thing, extended illumination will cause a noticeable temperature rise in the battery without any cooling device; then, the electrolyte will face constant evaporation through their porous cathodes, resulting in increased impedance and polarization. For another, aggressive photoelectrons/holes will directly attack the electrolyte and cause serious electrolyte decomposition. However, compared with the studies on photocathodes, much fewer efforts have been made in electrolytes for light-assisted metal–air batteries.

Aprotic electrolytes (LiTFSI/TEGDME) are widely utilized in light-assisted rechargeable Li–O_2 (CO_2) batteries due to their high boiling points, good chemical/electrochemical stability, and low cost. Researchers hold different views as to the influence of light on electrolyte stability. Some researchers proposed that the electrolytes face more serious degradation under illumination than in the dark.[62] Photocatalysis processes could result in the degradation of diluted ether electrolyte (1:1 mole ratio of LiTFSI: TEGDME) with distinct by-products shown in Raman and nuclear magnetic resonance spectra.[68] Introducing a super-concentrated electrolyte (4:1 mole ratio of LiTFSI: TEGDME) enhanced stability against unfavorable photocatalytic decomposition, and the battery durability was further ensured by a conventional and light-assisted hybrid charge strategy. By contrast, some studies proposed that electrolyte stability can be ensured under illumination due to the reduced polarization[64,71] or the accelerated transformation of aggressive intermediates under illumination,[80] in sharp contrast with the intensive electrolyte decomposition in the dark. Besides, some researchers pointed out that light has a limited influence on electrolyte stability. The ether electrolytes remained stable upon cycling under light, similar to those in the dark.[58,72] The above inconsistent conclusions can be associated with different electrolytes, photocatalysts, setups (e.g., coin cells, Swagelok cells, electrolyzer cells, or three-electrode cells), current densities, and temperatures in the different studies. For example, the interference of light on electrolytes will be limited to the batteries with excess electrolytes and operating at low current densities and low light intensities. Recently, light-assisted batteries with redox mediators have been reported to have superior stability because more holes would be consumed by the oxidation reactions of iodide ions instead of attacking the electrolyte.[76]

Solid-state electrolytes are considered more suitable choices than liquid electrolytes for open light-assisted battery systems due to their better photo/thermal/chemical stability. Li_2O–Al_2O_3–GeO_2–P_2O_5 (LAGP) electrolytes have been used in photothermal promoted Li–air batteries, which could bear the extremely high temperature up to 120 °C.[55,117] Besides, the LAGP electrolyte was also used in hybrid light-assisted Li–O_2 batteries to isolate the Li anode from the aqueous alkaline catholyte.[52,66] Considering that all-solid electrolytes present poor mechanical performance, low ionic conductivity, and large interfacial resistance, plastic-crystal electrolytes were introduced to achieve a flexible light-assisted Li-ion O_2 battery due to their excellent plasticity and high ionic conductivity.[53,139] Aqueous electrolytes (composed of water, base, and supporting salts) are commonly used in light-assisted Zn–air and hybrid Li–O_2 batteries; their stability has not been studied yet. Meanwhile, gel electrolytes have also been explored for light-assisted Zn–air batteries owing to their mechanical stability and safety.[99]

5. Challenges and Perspectives

In this Review, the configurations and mechanisms of light-assisted metal–air batteries have been discussed. Design strategies and specific examples of photocathodes have been systematically summarized. Finally, the influence of illumination on the whole batteries also has been carefully analyzed. Although light-assisted metal–air batteries have achieved important advances in recent years, many challenges remain to be tackled in future studies (Figure 8).

1) Light-assisted metal–air batteries still remain at the conception stage and need substantial efforts to meet practical performance requirements. First, most of reported devices present poor rate capability (operate at 0.01 $mA\,cm^{-2}$) and short lifespan (< 50 cycles) under illumination due to the limited light absorption, severe carrier recombination, and poor electrocatalytic activity of photocatalysts, while the huge interfacial resistance between photocatalyst and current collector further exacerbates this issue. Rationally designing the structure of photocathodes (e.g., the morphology and band structure of photocatalysts, the interface between photocatalysts and current collector) is essential for effective charge transfer and separation. Besides, introducing an external field (e.g., magnetic field, thermal gradient, mechanical stress, and acoustic waves) is also feasible to accelerate the photoelectrochemical processes in light-assisted batteries, which is still rarely explored. Improving the stability of electrolytes and anodes is also vital to the cycle life of the battery under illumination. Second, most batteries only demonstrate obviously decreased either charge or discharge overpotential but limited enhancement to another process, which is related to the carrier type of semiconductor photocatalysts. It is essential to develop photocatalysts to simultaneously promote discharge and charge processes or rationally integrate two photocatalysts into a photocathode. Utilizing two separate photocathodes in a light-assisted battery can be feasible, but this will lead to a complex

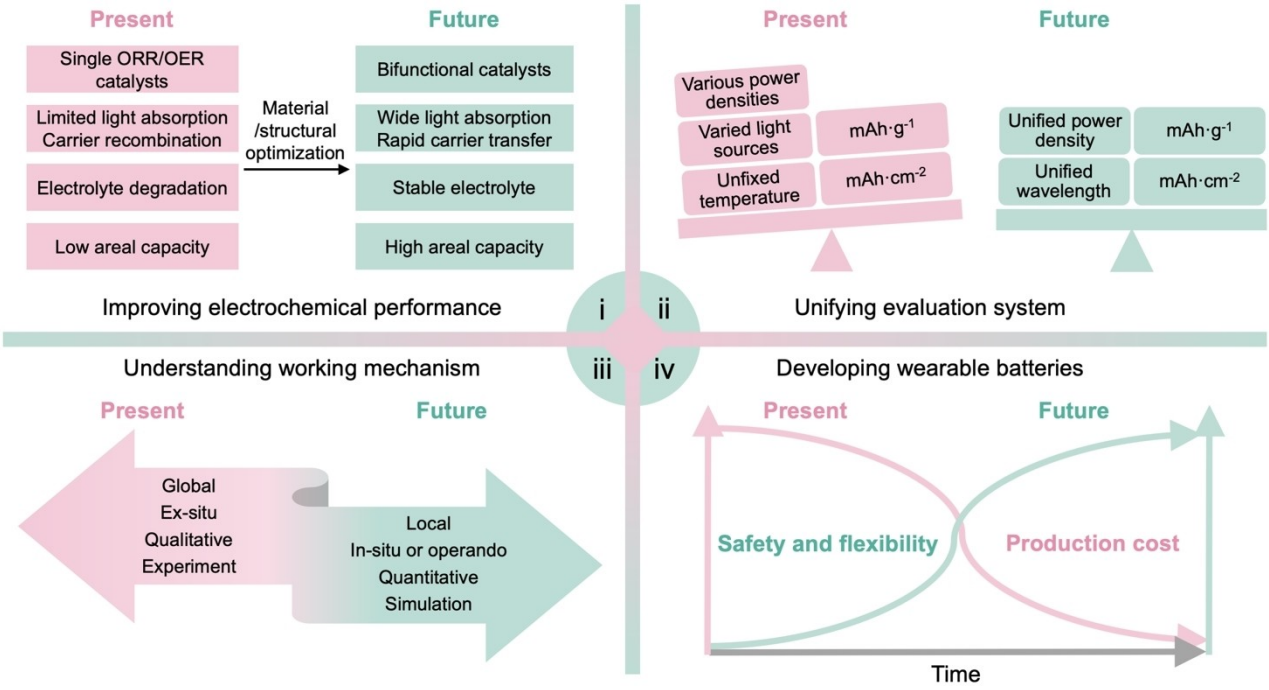

Figure 8. Present challenges and future perspectives of light-assisted metal–air batteries.

configuration and operation. Studies in the photocatalysis field will provide valuable experience for the design of photocathodes.[103,144,145] Different from the reported light-rechargeable Zn–ion batteries and capacitors,[146,147] light just makes a limited contribution to the practical current density in metal–air batteries, which still need to be charged at an external bias voltage due to the sluggish OER (CO_2ER) kinetics. Realizing real rechargeability at a zero bias voltage is an exciting but highly challenging research topic. This involves improving the reversibility of metal–air batteries through material and device design combined with special operating strategies.

2) It is difficult to compare light-assisted metal–air batteries due to the lack of standardized measurement conditions and methods. On the one hand, light-assisted batteries are fabricated in different forms (e.g., coin cells, electrolyzers, or Swagelok cells) and illuminated by various light sources with different wavelength ranges and power densities. Obviously, excess electrolyte or high-power illumination will lead to better battery performance. On the other hand, current densities ($mA\,cm^{-2}$, $mA\,g^{-1}$) and specific capacities ($mAh\,cm^{-2}$, $mAh\,g^{-1}$) on area or mass are adopted depending on what researchers want to emphasize. They can be calculated from a single photocatalyst, a whole electrode, or even an entire device. The above issues make it difficult to compare the reported battery performances. A unified and fair assessment standard is necessary to compare the constructed devices better. Currently, the term "energy efficiency" is adopted to describe the conversion efficiency of electric energy during discharging and charging processes with a cut-off capacity for regular metal–air batteries, but it can be confusing and inappropriate to use this term to describe metal–air batteries involving the conversion and storage of light energy. Instead, the term "round-trip efficiency" is considered more appropriate, while "energy efficiency" should refer to the conversion efficiency of photoenergy to electric energy in a light-assisted metal–air battery.

3) The working mechanisms of light-assisted metal–air batteries have not yet been clarified. Rechargeable metal–air batteries involve multistep chemical and electrochemical processes during discharging/charging, which become more complex with illumination. Current studies mainly focus on developing new photocatalysts for metal–air batteries and provide similar explanations of the discharge/charge processes of light-assisted metal–air batteries based on different photocatalysts, but lack in-depth insight into the fundamental photochemical and electrochemical processes. The following questions should be carefully concerned to understand light-assisted metal–air batteries better. How are the charge carriers generated, separated, transferred, recombined, and utilized at the photocathodes? Are the light-assisted discharge and charge processes really thermodynamically reversible? How does the reversibility vary with operating conditions (e.g., current density, illumination intensity, atmosphere, or temperature)? How does light influence the thermodynamic/kinetic behavior and long-term stability of the battery? An in-depth understanding of reaction mechanisms will lead to the rational material and structural design of light-assisted batteries. Drawing from photocatalysis and metal–air batteries, many advanced characterization methods (e.g., in situ Raman, X-ray diffraction, Fourier transform infrared, nuclear magnetic resonance spectroscopy, and differential elec-

trochemical mass spectrometry) can be utilized to discern the reaction mechanisms. For example, determining the generation of intermediates ($^1O_2$, O_2^-, $C_2O_4^{2-}$) or parasitic products (Li_2CO_3) and quantifying the consumption/evolution of gas molecules (O_2, CO_2) during discharging/charging under illumination is important to evaluate the real photo-involved battery performance. Theoretical analysis tools such as density functional theory can help predict or understand the specific reaction pathways at photocatalysts at the atom scale.[148] Only in this way we can better understand and then design the materials and configurations of light-assisted batteries.

4) Future studies should be devoted to more practical light-assisted metal–air batteries. Lowering production cost is essential for practical application, achieved by utilizing sustainable reagents/materials, compact configurations, and facile fabrication while retaining decent performance. Currently, most light-assisted batteries can only deliver excellent performance under illumination but poor performance in the dark. The batteries tolerating natural or even dam light should be designed in the future, which requires photocathodes with superior photocatalytic and electrocatalytic activity in the meantime. To meet requirements for wearable electronics, future batteries are expected to be safe, lightweight, flexible, and cheap, besides having decent electrochemical performance. Quasi-solid or all-solid electrolytes are better than liquid ones which are prone to volatilization and leakage in open metal–air batteries. Developing soft and lightweight materials to replace hard and brittle materials is vital to constructing flexible batteries, while designing batteries in fiber/fabric configurations is also a feasible route to achieve high flexibility. Designing lightweight, soft, transparent, and air-permeable packaging materials can be necessary. More efforts need to be made to explore possible applications of light-assisted batteries. Light-assisted metal–air batteries can find significant applications at special locations such as Mars. Integrating a light-assisted metal–air battery with other energy-storage devices is also promising for high-efficiency photoenergy harvesting and utilization.

Although light-assisted strategies have demonstrated enormous potential in achieving high-efficiency metal–air batteries, there are still many challenges in basic research and practical applications. As these challenges involve various research fields, including photochemistry, electrochemistry, materials, physics, and electronics, it is essential to invite scientists from multidisciplinary fields to work together to solve the above problems. We expect this Review to inspire more researchers and shape future research activities. We believe that light-assisted metal–air batteries will approach their practical applications after extensive efforts to reshape human lifestyles and even transform production pathways in the future.

Acknowledgements

This work was supported by NSFC (52222310) and STCSM (20JC1414902, 21511104900).

Conflict of Interest

The authors declare no conflict of interest.

Data Availability Statement

Data sharing is not applicable to this article as no new data were created or analyzed in this study.

Keywords: Metal–Air Batteries · Photocathodes · Round-Trip Efficiency · Semiconductors

[1] D. Lin, Y. Liu, Y. Cui, *Nat. Nanotechnol.* **2017**, *12*, 194.
[2] L. Ma, T. Yu, E. Tzoganakis, K. Amine, T. Wu, Z. Chen, J. Lu, *Adv. Energy Mater.* **2018**, *8*, 1800348.
[3] K. Chen, D. Y. Yang, G. Huang, X. B. Zhang, *Acc. Chem. Res.* **2021**, *54*, 632.
[4] J. Fu, Z. P. Cano, M. G. Park, A. Yu, M. Fowler, Z. Chen, *Adv. Mater.* **2017**, *29*, 1604685.
[5] C. Jia, F. Zhang, L. She, Q. Li, X. He, J. Sun, Z. Lei, Z. Liu, *Angew. Chem. Int. Ed.* **2021**, *60*, 11257; *Angew. Chem.* **2021**, *133*, 11357.
[6] A. C. Luntz, B. D. McCloskey, *Chem. Rev.* **2014**, *114*, 11721.
[7] J. Lai, Y. Xing, N. Chen, L. Li, F. Wu, R. Chen, *Angew. Chem. Int. Ed.* **2020**, *59*, 2974; *Angew. Chem.* **2020**, *132*, 2994.
[8] T. Liu, J. P. Vivek, E. W. Zhao, J. Lei, N. Garcia-Araez, C. P. Grey, *Chem. Rev.* **2020**, *120*, 6558.
[9] X. Chen, Z. Zhou, H. E. Karahan, Q. Shao, L. Wei, Y. Chen, *Small* **2018**, *14*, 1801929.
[10] Y. Qiao, J. Yi, S. Wu, Y. Qiao, J. Yi, S. Wu, Y. Liu, S. Yang, P. He, H. Zhou, *Joule* **2017**, *1*, 359.
[11] X. Yu, A. Manthiram, *Small Struct.* **2020**, *1*, 2000027.
[12] Z. Wang, D. Xu, J. Xu, X. Zhang, *Chem. Soc. Rev.* **2014**, *43*, 7746.
[13] H. Wang, Q. Xu, *Matter* **2019**, *1*, 565.
[14] F. Meng, K. Liu, Y. Zhang, M. Shi, X. Zhang, J. Yan, *Small* **2018**, *14*, 1703843.
[15] Z. Peng, S. A. Freunberger, Y. Chen, P. G. Bruce, *Science* **2012**, *337*, 563.
[16] J. Lu, Y. J. Lee, X. Luo, K. C. Lau, M. Asadi, H.-H. Wang, S. Brombosz, J. Wen, D. Zhai, Z. Chen, D. J. Miller, Y. S. Jeong, J.-B. Park, Z. Z. Fang, B. Kumar, A. Salehi-Khojin, Y.-K. Sun, L. A. Curtiss, K. Amine, *Nature* **2016**, *529*, 377.
[17] Y. Xing, Y. Yang, D. Li, M. Luo, N. Chen, Y. Ye, J. Qian, L. Li, D. Yang, F. Wu, S. Guo, *Adv. Mater.* **2018**, *30*, 1803124.
[18] L. Ma, N. Meng, Y. Zhang, F. Lian, *Nano Energy* **2019**, *58*, 508.
[19] P. Wang, Y. Ren, R. Wang, P. Zhang, M. Ding, C. Li, D. Zhao, Z. Qian, Z. Zhang, L. Zhang, L. Yin, *Nat. Commun.* **2020**, *11*, 1576.
[20] X. Li, J. Zhou, J. Zhang, M. Li, J. Cheng, F. Zhang, Y. Li, X. Mu, J. Lu, B. Wang, *Adv. Mater.* **2019**, *31*, 1903852.
[21] L. Qie, Y. Lin, J. W. Connell, J. Xu, L. Dai, *Angew. Chem. Int. Ed.* **2017**, *56*, 6970; *Angew. Chem.* **2017**, *129*, 7074.
[22] H. D. Lim, H. Song, J. Kim, H. Gwon, Y. Bae, K. Y. Park, J. Hong, H. Kim, T. Kim, Y. H. Kim, X. Leprõ, R. Ovalle-

Robles, R. H. Baughman, K. Kang, *Angew. Chem. Int. Ed.* **2014**, *53*, 3926; *Angew. Chem.* **2014**, *126*, 4007.
[23] L. Wang, J. Pan, Y. Zhang, X. Cheng, L. Liu, H. Peng, *Adv. Mater.* **2018**, *30*, 1704378.
[24] X. Wang, C. Wang, Z. Xie, X. Zhang, Y. Chen, D. Wu, *ChemElectroChem* **2017**, *4*, 2145.
[25] Y. Chen, S. A. Freunberger, Z. Peng, O. Fontaine, P. G. Bruce, *Nat. Chem.* **2013**, *5*, 489.
[26] B. J. Bergner, A. Schürmann, K. Peppler, A. Garsuch, J. Janek, *J. Am. Chem. Soc.* **2014**, *136*, 15054.
[27] G. Leverick, M. Tułodziecki, R. Tatara, F. Bardé, Y. Shao-Horn, *Joule* **2019**, *3*, 1106.
[28] M. Yu, X. Ren, Y. Wu, *Nat. Commun.* **2014**, *5*, 5111.
[29] Q. Li, Y. Liu, S. Guo, H. Zhou, *Nano Today* **2017**, *16*, 46.
[30] A. Gurung, Q. Qiao, *Joule* **2018**, *2*, 1217.
[31] M. Yu, W. D. McCulloch, Z. Huang, B. B. Trang, J. Lu, K. Amine, Y. Wu, *J. Mater. Chem. A* **2016**, *4*, 2766.
[32] Z. Fang, X. Hu, D. Yu, *ChemPlusChem* **2020**, *85*, 600.
[33] N. Yan, X. Gao, *Energy Environ. Mater.* **2022**, *5*, 439.
[34] Q. Zeng, Y. Lai, L. Jiang, F. Liu, X. Hao, L. Wang, M. A. Green, *Adv. Energy Mater.* **2020**, *10*, 1903930.
[35] P. Tan, X. Xiao, Y. Dai, C. Cheng, M. Ni, *Renewable Sustainable Energy Rev.* **2020**, *127*, 109877.
[36] D. Du, Z. Zhu, K.-Y. Chan, F. Li, J. Chen, *Chem. Soc. Rev.* **2022**, *51*, 1846.
[37] Y. Ma, X. Wang, Y. Jia, X. Chen, H. Han, C. Li, *Chem. Rev.* **2014**, *114*, 9987.
[38] S. Wang, L. Chen, X. Zhao, J. Zhang, Z. Ao, W. Liu, H. Wu, L. Shi, Y. Yin, X. Xu, C. Zhao, X. Duan, S. Wang, H. Sun, *Appl. Catal. B* **2020**, *278*, 119312.
[39] B. Ma, G. Chen, C. Fave, L. Chen, R. Kuriki, K. Maeda, O. Ishitani, T. C. Lau, J. Bonin, M. Robert, *J. Am. Chem. Soc.* **2020**, *142*, 6188.
[40] Y. Wang, X. Wang, M. Antonietti, *Angew. Chem. Int. Ed.* **2012**, *51*, 68; *Angew. Chem.* **2012**, *124*, 70.
[41] B. Wu, L. Zhang, B. Jiang, Q. Li, C. Tian, Y. Xie, W. Li, H. Fu, *Angew. Chem. Int. Ed.* **2021**, *60*, 4815; *Angew. Chem.* **2021**, *133*, 4865.
[42] P. Zhang, Y. Zhao, *Chem. Soc. Rev.* **2018**, *47*, 2921.
[43] K. Chen, G. Huang, J. Ma, J. Wang, D. Yang, X. Yang, Y. Yua, X. Zhang, *Angew. Chem. Int. Ed.* **2020**, *59*, 16661; *Angew. Chem.* **2020**, *132*, 16804.
[44] D. Wang, X. Mu, P. He, H. Zhou, *Mater. Today* **2019**, *26*, 87.
[45] J. Pan, Y. Y. Xu, H. Yang, Z. Dong, H. Liu, B. Y. Xia, *Adv. Sci.* **2018**, *5*, 1700691.
[46] L. Li, Y. C. A. Tsang, D. Xiao, G. Zhu, C. Zhi, Q. Chen, *Nat. Commun.* **2022**, *13*, 2870.
[47] H. Li, L. Ma, C. Han, Z. Wang, Z. Liu, Z. Tang, C. Zhi, *Nano Energy* **2019**, *62*, 550.
[48] X. Mu, H. Pan, P. He, H. Zhou, *Adv. Mater.* **2020**, *32*, 1903790.
[49] X. Li, S. Yang, N. Feng, P. He, H. Zhou, *Chin. J. Catal.* **2016**, *37*, 1016.
[50] M. Balaish, J. W. Jung, I. D. Kim, Y. Ein-Eli, *Adv. Funct. Mater.* **2020**, *30*, 1808303.
[51] X. Liu, Y. Yuan, J. Liu, et al., *Nat. Commun.* **2019**, *10*, 4767.
[52] H. Gong, H. Xue, B. Gao, Y. Li, X. Fan, S. Zhang, T. Wang, J. He, *Energy Storage Mater.* **2020**, *31*, 11.
[53] Y. Liu, J. Yi, Y. Qiao, D. Wang, P. He, Q. Li, S. Wu, H. Zhou, *Energy Storage Mater.* **2018**, *11*, 170.
[54] D. Guan, X. Wang, M. Li, F. Li, L. Zheng, X. Huang, J. Xu, *Angew. Chem. Int. Ed.* **2020**, *59*, 19518; *Angew. Chem.* **2020**, *132*, 19686.
[55] H. Song, S. Wang, X. Song, J. Wang, K. Jiang, S. Huang, M. Han, J. Xu, P. He, K. Chen, H. Zhou, *Energy Environ. Sci.* **2020**, *13*, 1205.
[56] Y. Liu, N. Li, S. Wu, K. Liao, K. Zhu, J. Yi, H. Zhou, *Energy Environ. Sci.* **2015**, *8*, 2664.
[57] Y. Liu, N. Li, K. Liao, Q. Li, M. Ishida, H. Zhou, *J. Mater. Chem. A* **2016**, *4*, 12411.
[58] Z. Zhu, Y. Ni, Q. Lv, J. Geng, W. Xie, F. Li, J. Chen, *Proc. Natl. Acad. Sci. USA* **2021**, *118*, e2024619118.
[59] F. Li, M. Li, H. Wang, X. Wang, L. Zheng, D. Guan, L. Chang, J. Xu, Y. Wang, *Adv. Mater.* **2022**, *34*, 2107826.
[60] X. Liu, S. Tao, J. Zhang, Y. Zhu, R. Ma, J. Lu, *J. Mater. Chem. A* **2021**, *9*, 26061.
[61] H. Gong, T. Wang, H. Xue, X. Fan, B. Gao, H. Zhang, L. Shi, J. He, J. Ye, *Energy Storage Mater.* **2018**, *13*, 49.
[62] M. Li, X. Wang, F. Li, L. Zheng, J. Xu, J. Yu, *Adv. Mater.* **2020**, *32*, 1907098.
[63] X. Yang, X. Feng, X. Jin, M. Shao, B. Yan, J. Yan, Y. Zhang, X. Zhang, *Angew. Chem. Int. Ed.* **2019**, *58*, 16411; *Angew. Chem.* **2019**, *131*, 16563.
[64] S. Tong, C. Luo, J. Li, Z. Mei, M. Wu, A. P. O'Mullane, H. Y. Zhu, *Angew. Chem. Int. Ed.* **2020**, *59*, 20909; *Angew. Chem.* **2020**, *132*, 21095.
[65] Y. Feng, H. Xue, T. Wang, H. Gong, B. Gao, W. Xia, C. Jiang, J. Li, X. Huang, J. He, *ACS Sustainable Chem. Eng.* **2019**, *7*, 5931.
[66] H. Gong, H. Xue, B. Gao, Y. Li, X. Yu, X. Fan, S. Zhang, T. Wang, J. He, *Chem. Commun.* **2020**, *56*, 13642.
[67] X. Yu, H. Gong, B. Gao, X. Fan, P. Li, X. Huang, K. Chang, T. Wang, J. He, *Chem. Eng. J.* **2022**, *449*, 137774.
[68] Y. Qiao, Y. Liu, K. Jiang, X. Li, Y. He, Q. Li, S. Wu, H. Zhou, *Small Methods* **2018**, *2*, 1700284.
[69] V. Veeramani, Y. Chen, H. Wang, T. Hung, *Chem. Eng. J.* **2018**, *349*, 235.
[70] H. Gong, T. Wang, K. Chang, P. Li, L. Liu, X. Yu, B. Gao, H. Xue, R. Ma, J. He, J. Ye, *Carbon Energy* **2022**, https://doi.org/10.1002/cey2.208.
[71] D. Li, X. Lang, Y. Guo, Y. Wang, Y. Wang, H. Shi, S. Wu, W. Wang, Q. H. Yang, *Nano Energy* **2021**, *85*, 105966.
[72] Z. Zhu, X. Shi, G. Fan, F. Li, J. Chen, *Angew. Chem. Int. Ed.* **2019**, *58*, 19021; *Angew. Chem.* **2019**, *131*, 19197.
[73] S. Kumar, A. Jena, C. Hu, C. Liang, W. Zhou, T. Hung, W. Chang, H. Chang, R. Liu, *ChemElectroChem* **2018**, *5*, 29.
[74] Z. Zhu, Q. Lv, Y. Ni, S. Gao, J. Geng, J. Liang, F. Li, *Angew. Chem. Int. Ed.* **2022**, *61*, e202116699; *Angew. Chem.* **2022**, *134*, e202116699.
[75] Q. Lv, Z. Zhu, S. Zhao, L. Wang, Q. Zhao, F. Li, L. A. Archer, J. Chen, *J. Am. Chem. Soc.* **2021**, *143*, 1941.
[76] W. Liu, Y. Yang, X. Hu, Q. Zhang, C. Wang, J. Wei, Z. Xie, Z. Zhou, *Small* **2022**, *18*, 2200334.
[77] G. Y. Qiao, D. Guan, S. Yuan, H. Rao, X. Chen, J. A. Wang, J. S. Qin, J. J. Xu, J. Yu, *J. Am. Chem. Soc.* **2021**, *143*, 14253.
[78] R. Fan, Y. Wu, H. Xie, Y. Gao, L. Wang, B. Zhao, D. Li, S. Liu, Y. Zhang, H. Kong, Y. Li, Q. Chen, A. Cao, H. Zhou, *ChemSusChem* **2022**, *15*, e202201473.
[79] F. Li, L. Zheng, X. Wang, M. Li, J. Xu, Y. Wang, *ACS Appl. Mater. Interfaces* **2021**, *13*, 26123.
[80] L. Zheng, F. Li, L. Song, M. Li, X. Wang, J. Xu, *Energy Storage Mater.* **2021**, *42*, 618.
[81] X. Wang, D. Guan, F. Li, M. Li, L. Zheng, J. Xu, *Adv. Mater.* **2022**, *34*, 2104792.
[82] X. X. Wang, D. H. Guan, F. Li, M. L. Li, L. J. Zheng, J. J. Xu, *Small* **2021**, *17*, 2100642.
[83] C. Wang, Y. Shang, Y. Lu, L. Qu, H. Yao, Z. Li, Q. Liu, *J. Power Sources* **2020**, *475*, 228703.
[84] K. Zhang, J. Li, W. Zhai, C. Li, Z. Zhu, X. Kang, M. Liao, L. Ye, T. Kong, C. Wang, Y. Zhao, P. Chen, Y. Gao, B. Wang, H. Peng, *Angew. Chem. Int. Ed.* **2022**, *61*, e202201718; *Angew. Chem.* **2022**, *134*, e202201718.

[85] A. Jena, H. Hsieh, S. Thoka, S. Hu, H. Chang, R. Liu, *ChemSusChem* **2020**, *13*, 2719.

[86] J. Li, K. Zhang, Y. Zhao, C. Wang, L. Wang, L. Wang, M. Liao, L. Ye, Y. Zhang, Y. Gao, B. Wang, H. Peng, *Angew. Chem. Int. Ed.* **2022**, *61*, e202114612; *Angew. Chem.* **2022**, *134*, e202114612.

[87] Z. Li, M. Li, X. Wang, D. Guan, W. Liu, J. Xu, *J. Mater. Chem. A* **2020**, *8*, 14799.

[88] S. Wang, H. Song, T. Zhu, J. Chen, Z. Yu, P. Wang, L. Yu, J. Xu, H. Zhou, K. Chen, *Nano Energy* **2022**, *100*, 107521.

[89] D. H. Guan, X. X. Wang, F. Li, L. J. Zheng, M. L. Li, H. F. Wang, J. J. Xu, *ACS Nano* **2022**, *16*, 12364.

[90] C. Tomon, S. Sarawutanukul, S. Duangdangchote, A. Krittayavathananon, M. Sawangphruk, *Chem. Commun.* **2019**, *55*, 5855.

[91] S. Sarawutanukul, C. Tomon, S. Duangdangchote, N. Phattharasupakun, M. Sawangphruk, *Batteries Supercaps* **2020**, *3*, 541.

[92] J. Lv, S. C. Abbas, Y. Huang, Q. Liu, M. Wu, Y. Wang, L. Dai, *Nano Energy* **2018**, *43*, 130.

[93] D. Bu, M. Batmunkh, Y. Zhang, Y. Li, B. Qian, Y. Lan, X. Hou, S. Li, B. Jia, X. M. Song, T. Ma, *Chem. Eng. J.* **2022**, *433*, 133559.

[94] H. Feng, C. Zhang, Z. Liu, J. Sang, S. Xue, P. K. Chu, *Chem. Eng. J.* **2022**, *434*, 134650.

[95] Z. Fang, Y. Li, J. Li, C. Shu, L. Zhong, S. Lu, C. Mo, M. Yang, D. Yu, *Angew. Chem. Int. Ed.* **2021**, *60*, 17615; *Angew. Chem.* **2021**, *133*, 17756.

[96] X. Wang, Y. Li, M. Yang, C. Liu, J. Li, D. Yu, *Adv. Funct. Mater.* **2022**, *32*, 2205518.

[97] D. Zhu, Q. Zhao, G. Fan, S. Zhao, L. Wang, F. Li, *Angew. Chem. Int. Ed.* **2019**, *58*, 12460; *Angew. Chem.* **2019**, *131*, 12590.

[98] D. Du, S. Zhao, Z. Zhu, F. Li, J. Chen, *Angew. Chem. Int. Ed.* **2020**, *59*, 18140; *Angew. Chem.* **2020**, *132*, 18297.

[99] Z. Fang, Y. Zhang, X. Hu, X. Fu, L. Dai, D. Yu, *Angew. Chem. Int. Ed.* **2019**, *58*, 9248; *Angew. Chem.* **2019**, *131*, 9349.

[100] X. Hou, Y. Zhang, C. Cui, C. Lin, Y. Li, D. Bu, G. Yan, D. Liu, Q. Wu, X. M. Song, *J. Power Sources* **2022**, *533*, 231377.

[101] J. Liu, N. Ma, W. Wu, Q. He, *Chem. Eng. J.* **2020**, *393*, 124719.

[102] J. Low, J. Yu, M. Jaroniec, S. Wageh, A. A. Al-Ghamdi, *Adv. Mater.* **2017**, *29*, 1601694.

[103] C. Hu, S. Tu, N. Tian, T. Ma, Y. Zhang, H. Huang, *Angew. Chem. Int. Ed.* **2021**, *60*, 16309; *Angew. Chem.* **2021**, *133*, 16445.

[104] J. Schneider, M. Matsuoka, M. Takeuchi, J. Zhang, Y. Horiuchi, M. Anpo, D. W. Bahnemann, *Chem. Rev.* **2014**, *114*, 9919–9986.

[105] J. Han, S. Lee, C. Youn, J. Lee, Y. Kim, T. Choi, *Electrochim. Acta* **2020**, *332*, 135443.

[106] H. Xue, T. Wang, Y. Feng, H. Gong, X. Fan, B. Gao, Y. Kong, C. Jiang, S. Zhang, X. Huang, J. He, *Nanoscale* **2020**, *12*, 18742.

[107] X. Wang, K. Maeda, A. Thomas, K. Takanabe, G. Xin, J. M. Carlsson, K. Domen, M. Antonietti, *Nat. Mater.* **2009**, *8*, 76.

[108] W. Ong, L. Tan, Y. H. Ng, S. Yong, S. Chai, *Chem. Rev.* **2016**, *116*, 7159.

[109] T. Y. Ma, S. Dai, M. Jaroniec, S. Z. Qiao, *Angew. Chem. Int. Ed.* **2014**, *53*, 7281; *Angew. Chem.* **2014**, *126*, 7409.

[110] P. Zhai, T. Wang, H. Jiang, J. Wan, Y. Wei, L. Wang, W. Liu, Q. Chen, W. Yang, Y. Cui, Y. Gong, *Adv. Mater.* **2021**, *33*, 2006247.

[111] L. Chen, R. Yan, M. Oschatz, L. Jiang, M. Antonietti, K. Xiao, *Angew. Chem. Int. Ed.* **2020**, *59*, 9067; *Angew. Chem.* **2020**, *132*, 9152.

[112] Y. Guo, P. Niu, Y. Liu, Y. Ouyang, D. Li, T. Zhai, *Adv. Mater.* **2019**, *31*, 1900342.

[113] L. Zhang, Z. Xu, B. Lou, L. Han, X. Zhang, *ChemSusChem* **2014**, *7*, 2427.

[114] B. Zhang, S. Wang, W. Fan, W. Ma, Z. Liang, J. Shi, *Angew. Chem. Int. Ed.* **2016**, *55*, 14748; *Angew. Chem.* **2016**, *128*, 14968.

[115] K. Wang, Z. Mo, S. Tang, M. Li, H. Yang, B. Long, *J. Mater. Chem. A* **2019**, *7*, 14129.

[116] J. Zhu, W. Nie, Q. Wang, W. Wen, X. Zhang, F. Li, S. Wang, *Chem. Commun.* **2020**, *56*, 5739.

[117] S. Wang, H. Song, X. Song, T. Zhu, Y. Ye, J. Chen, L. Yu, J. Xu, K. Chen, *Energy Storage Mater.* **2021**, *39*, 139.

[118] B. Liu, W. Xu, J. Zheng, P. Yan, E. D. Walter, N. G. Isern, M. E. Bowden, M. H. Engelhard, S. T. Kim, J. Read, B. D. Adams, X. Li, J. Cho, C. Wang, J.-G. Zhang, *ACS Energy Lett.* **2017**, *2*, 2525.

[119] J. Li, L. Wang, Y. Zhao, S. Li, X. Fu, B. Wang, H. Peng, *Adv. Funct. Mater.* **2020**, *30*, 2001619.

[120] X. Xie, Z. Fang, M. Yang, F. Zhu, D. Yu, *Adv. Funct. Mater.* **2021**, *31*, 2007942.

[121] L. D. Griffith, A. E. S. Sleightholme, J. F. Mansfield, D. J. Siegel, C. W. Monroe, *ACS Appl. Mater. Interfaces* **2015**, *7*, 7670.

[122] R. R. Mitchell, B. M. Gallant, Y. Shao-Horn, C. V. Thompson, *J. Phys. Chem. Lett.* **2013**, *4*, 1060.

[123] L. Johnson, C. Li, Z. Liu, Y. Chen, S. A. Freunberger, P. C. Ashok, B. B. Praveen, K. Dholakia, J. M. Tarascon, P. G. Bruce, *Nat. Chem.* **2014**, *6*, 1091.

[124] N. B. Aetukuri, B. D. McCloskey, J. M. Garciá, L. E. Krupp, V. Viswanathan, A. C. Luntz, *Nat. Chem.* **2015**, *7*, 50.

[125] Y. Qiao, S. Wu, J. Yi, Y. Sun, S. Guo, S. Yang, P. He, H. Zhou, *Angew. Chem. Int. Ed.* **2017**, *56*, 4960; *Angew. Chem.* **2017**, *129*, 5042.

[126] X. Chi, M. Li, J. Di, P. Bai, L. Song, X. Wang, F. Li, S. Liang, J. Xu, J. Yu, *Nature* **2021**, *592*, 551.

[127] L. N. Song, W. Zhang, Y. Wang, X. Ge, L. C. Zou, H. F. Wang, X. X. Wang, Q. C. Liu, F. Li, J. J. Xu, *Nat. Commun.* **2020**, *11*, 2191.

[128] P. Tan, W. Shyy, T. S. Zhao, Z. H. Wei, L. An, *J. Power Sources* **2015**, *278*, 133.

[129] B. M. Gallant, D. G. Kwabi, R. R. Mitchell, J. Zhou, C. V. Thompson, Y. Shao-Horn, *Energy Environ. Sci.* **2013**, *6*, 2518.

[130] B. D. Adams, C. Radtke, R. Black, M. L. Trudeau, K. Zaghib, L. F. Nazar, *Energy Environ. Sci.* **2013**, *6*, 1772.

[131] Y. Hu, X. Han, F. Cheng, Q. Zhao, Z. Hu, J. Chen, *Nanoscale* **2014**, *6*, 177.

[132] C. Shu, J. Wang, J. Long, H. K. Liu, S. X. Dou, *Adv. Mater.* **2019**, *31*, 1804587.

[133] Z. Zhao, E. Wang, J. Wang, C. Liu, Z. Peng, *J. Mater. Chem. A* **2021**, *9*, 3290.

[134] S. Chen, D. Huang, P. Xu, W. Xue, L. Lei, M. Cheng, R. Wang, X. Liu, R. Deng, *J. Mater. Chem. A* **2020**, *8*, 2286.

[135] Y. Wang, H. Shi, K. Cui, J. Yu, *Appl. Catal. B* **2019**, *250*, 171.

[136] G. Huang, J. Wang, X. Zhang, *ACS Cent. Sci.* **2020**, *6*, 2136.

[137] S. A. Freunberger, Y. Chen, N. E. Drewett, L. J. Hardwick, F. Bardø, P. G. Bruce, *Angew. Chem. Int. Ed.* **2011**, *50*, 8609; *Angew. Chem.* **2011**, *123*, 8768.

[138] M. Asadi, B. Sayahpour, P. Abbasi, A. T. Ngo, K. Karis, J. R. Jokisaari, C. Liu, B. Narayanan, M. Gerard, P. Yasaei, X. Hu, A. Mukherjee, K. C. Lau, R. S. Assary, F. Khalili-Araghi, R. F. Klie, L. A. Curtiss, A. Salehi Khojin, *Nature* **2018**, *555*, 502.

[139] J. Wang, G. Huang, K. Chen, X.-B. Zhang, *Angew. Chem. Int. Ed.* **2020**, *59*, 9382; *Angew. Chem.* **2020**, *132*, 9468.

[140] B. D. Adams, R. Black, Z. Williams, R. Fernandes, M. Cuisinier, E. J. Berg, P. Novak, G. K. Murphy, L. F. Nazar, *Adv. Energy Mater.* **2015**, *5*, 1400867.
[141] Z. Huang, H. Zeng, M. Xie, X. Lin, Z. Huang, Y. Shen, *Angew. Chem. Int. Ed.* **2019**, *58*, 2345; *Angew. Chem.* **2019**, *131*, 2367.
[142] F. Li, T. Zhang, Y. Yamada, A. Yamada, H. Zhou, *Adv. Energy Mater.* **2013**, *3*, 532.
[143] B. Liu, W. Xu, P. Yan, X. Sun, M. E. Bowden, J. Read, J. Qian, D. Mei, C. Wang, J. Zhang, *Adv. Funct. Mater.* **2016**, *26*, 605.
[144] X. Li, W. Wang, F. Dong, Z. Zhang, L. Han, X. Luo, J. Huang, Z. Feng, Z. Chen, G. Jia, T. Zhang, *ACS Catal.* **2021**, *11*, 4739.
[145] W. Gao, J. Lu, S. Zhang, X. Zhang, Z. Wang, W. Qin, J. Wang, W. Zhou, H. Liu, Y. Sang, *Adv. Sci.* **2019**, *6*, 1901244.
[146] B. Deka Boruah, A. Mathieson, S. K. Park, X. Zhang, B. Wen, L. Tan, A. Boies, M. De Volder, *Adv. Energy Mater.* **2021**, *11*, 2100115.
[147] B. D. Boruah, A. Mathieson, B. Wen, C. Jo, F. Deschler, M. De Volder, *Nano Lett.* **2020**, *20*, 5967.
[148] T. He, Y. Chen, Q. Liu, B. Lu, X. Song, H. Liu, M. Liu, Y. N. Liu, Y. Zhang, X. Ouyang, S. Chen, *Angew. Chem. Int. Ed.* **2022**, *61*, e202201007; *Angew. Chem.* **2022**, *134*, e202201007.

Manuscript received: September 3, 2022
Accepted manuscript online: October 5, 2022
Version of record online: November 10, 2022